Contributions of mechanical loading and hormonal changes to eccentric hypertrophy during volume overload: a Bayesian analysis using logic-based network models.

Johane H. Bracamonte[1], Lionel Watkins[2], Pat Betty[3,4], Louis J. Dell'Italia[3,4], Jeffrey J. Saucerman[2], Jeffrey W. Holmes[1,*]

(1) Department of Biomedical Engineering, University of Alabama at Birmingham, Birmingham, Alabama, United States of America.

(2) Department of Biomedical Engineering, University of Virginia, Charlottesville, Virginia, United States of America.

(3) Birmingham Veterans Affairs Health Care System, Birmingham, Alabama, United States of America.

(4) Division of Cardiovascular Disease, Heersink School of Medicine, University of Alabama at Birmingham, Birmingham, Alabama, United States of America.

(*) Corresponding author. Email: holmesjw@uab.edu

Author Summary

Mitral valve regurgitation is a common heart disease in which a malfunctioning valve allows part of the blood pumped by the heart to flow in the wrong direction. This condition overloads the heart by making it pump more blood volume than normal; the heart temporarily adapts by growing in mass and volume, but if untreated the condition can ultimately lead to heart failure and death. The most effective treatment is to surgically repair the valve; however, in many patients heart function deteriorates even after a successful surgery. Many researchers have studied this condition by experimentally overloading the hearts of dogs and rats, producing large amounts of data on the resulting geometric, mechanical, and biologic changes. Yet there is no clear answer on how to prevent the progression of the disease. In this work we integrate experimental data reported from 70 research articles on experimental volume overload through a simple model of heart mechanics and a more complex model of the molecular signaling pathways inside heart cells. We use a statistical approach to calibrate the computational model, so that it can predict not only average responses but also the degree of expected uncertainty for each prediction. We then use the model to explore how the heart responds to potential treatments during overload.

Statements and Declarations

Funding:

This work is supported by the American Heart Association postdoctoral fellowship grant 23POST1026645 (https://doi.org/10.58275/AHA.23POST1026645.pc.gr.161204) to J.H.B; the National Institutes of Health and National Heart, Lung, and Blood Institute (NIH/NHLBI) grants R01HL159945 to J.W.H, R01HL162925 to J.J.S, and P01 HL051952 and P50HL077100 to L.J.D; Department of Veteran Affairs for Merit Review grant 1CX000993-01 to L.J.D, and Department of Veteran Affairs John B. Barnwell Award to L.J.D.

Competing interest:

The authors have no competing interests to declare that are relevant to the content of this article.

Availability of data and source codes:

Links to GitHub repositories containing all data and codes are provided within the text.

Authors contributions:

Conceptualization: Johane H. Bracamonte, Jeffrey W. Holmes

Data Curation: Johane H. Bracamonte, Betty Pat, Lou J. Dell'Italia

Formal Analysis: Johane H. Bracamonte, Lionel Watkins

Funding Acquisition: Johane H. Bracamonte, Jeffrey W. Holmes, Jeffrey J. Saucerman, Lou J. Dell'Italia

Investigation: Johane H. Bracamonte, Jeffrey W. Holmes, Betty Pat, Lou J. Dell'Italia

Methodology: Johane H. Bracamonte, Jeffrey W. Holmes, Jeffrey J. Saucerman

Project Administration: Jeffrey W. Holmes

Resources: Johane H. Bracamonte, Jeffrey W. Holmes, Jeffrey J. Saucerman, Betty Pat, Lou J. Dell'Italia

Software: Johane H. Bracamonte, Lionel Watkins, Jeffrey J. Saucerman

Supervision: Jeffrey W. Holmes

Validation: Johane H. Bracamonte, Jeffrey W. Holmes

Visualization: Johane H. Bracamonte, Lionel Watkins

Writing-original draft preparation: Johane H. Bracamonte

Writing-review and editing: Johane H. Bracamonte, Jeffrey W. Holmes, Jeffrey J. Saucerman, Lou J. Dell'Italia

Abstract

Primary mitral regurgitation (MR) is a pathology that alters mechanical loading on the left ventricle and induces a distinctive ventricular remodeling response known as eccentric hypertrophy. Drug therapies may alleviate symptoms, but only mitral valve repair can provide significant recovery of cardiac function and dimensions. However, 20% of patients still develop systolic dysfunction post-operatively despite being treated according to the current guidelines. Thus, better understanding of the hypertrophic process in the setting of ventricular volume overload (VO) is needed to improve and better personalize the management of MR. To address this knowledge gap, we employ a Bayesian approach to combine data from 70 studies on experimental volume overload in dogs and rats and use it to calibrate a logic-based network model of hypertrophic signaling in myocytes. The calibrated model suggests that growth in experimental VO is mostly driven by the neurohormonal response, with an initial increase in myocardial tissue stretch being compensated by subsequent remodeling fairly early in the time course of VO. This observation contrasts with a common perception that volume-overload hypertrophy is driven primarily by increased myocyte strain. The model suggests that Endothelin1 receptor activity plays a central role in driving hypertrophic responses and the activation of the fetal gene program. The model reproduces a number of responses to drug therapy not used in its calibration, and predicts that a combination of endothelin receptor antagonist and angiotensin receptor blockers would have the greatest potential to dampen cardiomyocyte hypertrophy and dysfunction in VO.

Author Summary

Mitral valve regurgitation is a common heart disease in which a malfunctioning valve allows part of the blood pumped by the heart to flow in the wrong direction. This condition overloads the heart by making it pump more blood volume than normal; the heart temporarily adapts by growing in mass and volume, but if untreated the condition can ultimately lead to heart failure and death. The most effective treatment is to surgically repair the valve; however, in many patients heart function deteriorates even after a successful surgery. Many researchers have studied this condition by experimentally overloading the hearts of dogs and rats, producing large amounts of data on the resulting geometric, mechanical, and biologic changes. Yet there is no clear answer on how to prevent the progression of the disease. In this work we integrate experimental data reported from 70 research articles on experimental volume overload through a simple model of heart mechanics and a more complex model of the molecular signaling pathways inside heart cells. We use a statistical approach to calibrate the computational model, so that it can predict not only average responses but also the degree of expected uncertainty for each prediction. We then use the model to explore how the heart responds to potential treatments during overload.

1. Introduction

Mitral valve regurgitation affects around 5 million people in America, and about 2% of the general population, with prevalence steeply increasing in individuals over 50 years of age [1]. In primary mitral regurgitation (MR) the dysfunction of one or more components of the valvular apparatus allows part of the blood volume pumped by the left ventricle to flow back to the low-pressure atrial compartment, making the heart pump a larger than usual volume of blood against a lower-than-normal resistance. The unique loading conditions imposed by MR induce a distinctive ventricular remodeling response known as eccentric hypertrophy, consisting of the lengthening of individual cardiomyocytes by addition of sarcomeres in series, leading to an organ-scale dilation of the left ventricle volume with little change in its wall thickness [2,3]. The neurohormonal response to volume overload is characterized by the activation of the sympathetic and renin-angiotensin systems, similar to other forms of cardiac overloading [4–6]. If MR is severe enough or if it remains untreated for long enough, the condition can transition from a compensated asymptomatic stage into irreversible heart failure with systolic dysfunction, a condition where the heart is unable to supply sufficient cardiac output to the body [7,8].

Drug therapies for heart failure due to primary MR alleviate symptoms and slow its progression, but only mitral valve repair can provide significant recovery of cardiac function and dimensions [2,9]. This fact has led clinicians to operate earlier in the national course of primary MR; yet 20% of patients still develop systolic dysfunction post-operatively despite being treated according to the current guidelines [10,11]. This fact highlights our incomplete understanding of eccentric hypertrophy due to primary

133 MR and its transition into systolic dysfunction and heart failure. A better understanding
134 of this process is needed to improve and better personalize the management of MR.
135 Most computational models of growth and remodeling during volume overload have
136 focused on the role of myocyte overstretch in driving eccentric hypertrophy [12,13]. By
137 contrast, molecular studies have shown reduced activity in stretch-sensitive myocyte
138 signaling pathways during experimental volume overload, the opposite of what would be
139 expected if remodeling is driven by stretch [14–18]. We hypothesized that this apparent
140 paradox might stem from complex interactions between hypertrophic signaling
141 pathways triggered by stretching and those that respond to other hormones and growth
142 factors known to be upregulated during volume overload.
143 Here, we employ a Bayesian approach to combine the wealth of available data on
144 experimental volume overload in dogs and rats using a logic-based network model of
145 hypertrophic signaling in myocytes, with the goal of better understanding the relative
146 influence of multiple factors that influence eccentric hypertrophy. We employed data
147 from 70 studies of experimental volume overload to estimate the probability distribution
148 of input parameters for a network model of hypertrophic signaling in cardiomyocytes
149 during volume overload, accounting for evolving levels of mechanical strain and
150 circulating hormones such as norepinephrine (NE), angiotensin II (AngII), and atrial
151 ANP and brain (BNP) natriuretic peptides. We then validated the ability of the calibrated
152 model to reproduce features of volume overload not included in the calibration, as well
153 as experimental responses to relevant independent experiments such as infusion of
154 hormones that induce myocyte hypertrophy.

155 The calibrated and validated model developed here represents a probabilistic, model-
156 driven meta-analysis of a large body of data on volume-overload hypertrophy, and as
157 such may be useful for screening future pharmacologic interventions [19]. We briefly
158 explored this potential by simulating several combinations of receptor blockades and
159 protein knockdowns to assess their effect on cardiomyocyte size in the setting of
160 volume overload. Our analysis suggests that elevated levels of circulating hormones
161 drive much of the hypertrophic response during late stages of experimental volume
162 overload, and that hormone-driven growth can reduce myocyte strain levels below
163 baseline despite elevated left ventricular volumes. These results contrast with the
164 assumption of most computational models that elevated myocyte stretch drives
165 eccentric hypertrophy but agree with much of the available molecular and signaling
166 data. A screen of potential pharmacological interventions suggests that a combination of
167 endothelin receptor antagonists and angiotensin receptor should have the potential to
168 reduce VO-induced hypertrophy. However, these simulations also identify situations
169 such as β adrenergic blockade where accurate predictions will require a multiscale
170 approach that considers both direct effects on hypertrophic signaling as well as indirect
171 effects through changes in mechanics and hemodynamics.

172 **2. Methods**

173 2.1. Data collection

174 We reviewed and collected data from 37 research articles on experimental mitral
175 regurgitation in dogs and 33 articles on experimental volume overload in rats by aorto-
176 caval shunt. All data employed for our quantitative analysis were reported as a mean
177 value and standard deviation, so we assumed a normal probability distribution function

178 (PDF) for all measurement-derived variables. For the estimation of myocardial stretch at
179 tissue scale, we focused on canine experiments to avoid confounding effects of growth
180 in body size and weight common during experimental volume overload in rodents. We
181 collected data on changes in left ventricular (LV) mass, end-diastolic volume (V_{ED}), and
182 free wall thickness (h_{ED}), as well as previously reported estimates of end-diastolic
183 myofiber stretch in healthy dogs (λ_{ED}^{0}).
184 Both experimental VO and naturally occurring MR in dogs trigger elevated circulating
185 levels of multiple hormones relevant to hypertrophic signaling, including AngII, NE, ET-
186 1, NE, ANP and BNP. We collected all data on plasma or serum concentrations of these
187 hormones reported in the reviewed articles. All these species correspond to input nodes
188 in the cardiomyocyte network model. We also collected data reported in the studies we
189 reviewed on activity and phosphorylation levels of intracellular signaling proteins from
190 Western blotting on myocardial tissue extractions at several stages of VO. Specifically,
191 we collected data on focal adhesion kinase (FAK), Akt, ERK5, ERK12, ELK1, cGMP,
192 p38, and JNK, corresponding to intermediate nodes in the cardiomyocyte signaling
193 model. Additionally, we collected data on the abundance of proteins that are
194 synthesized by myocytes in tissue samples extracted following chronic VO and
195 correspond to output nodes in the model, including SERCA, Myosin heavy chain
196 isoforms αMHC and βMHC, ANP and BNP [20].
197 A detailed list of sources for all the collected quantitative data is summarized in the
198 supplementary material S1.1.

199 ### 2.2. Integration of canine and rat experimental data

Plots of the experimental fold change of normalized LV mass to body mass (LVM/BM) during volume overload showed very similar shapes for dogs and rats, but hypertrophy occurred much faster in rats [8]. When we fitted data from each species with an exponential function and normalized the time axis by the time constant of that fit, we found that data from both species aligned (Fig 1a, the full list of data sources is shown in supplementary material S1.1). We therefore normalized all time course data in this study by the time constant for each species. This allowed the use of combined data from both animal models in our quantitative analysis.

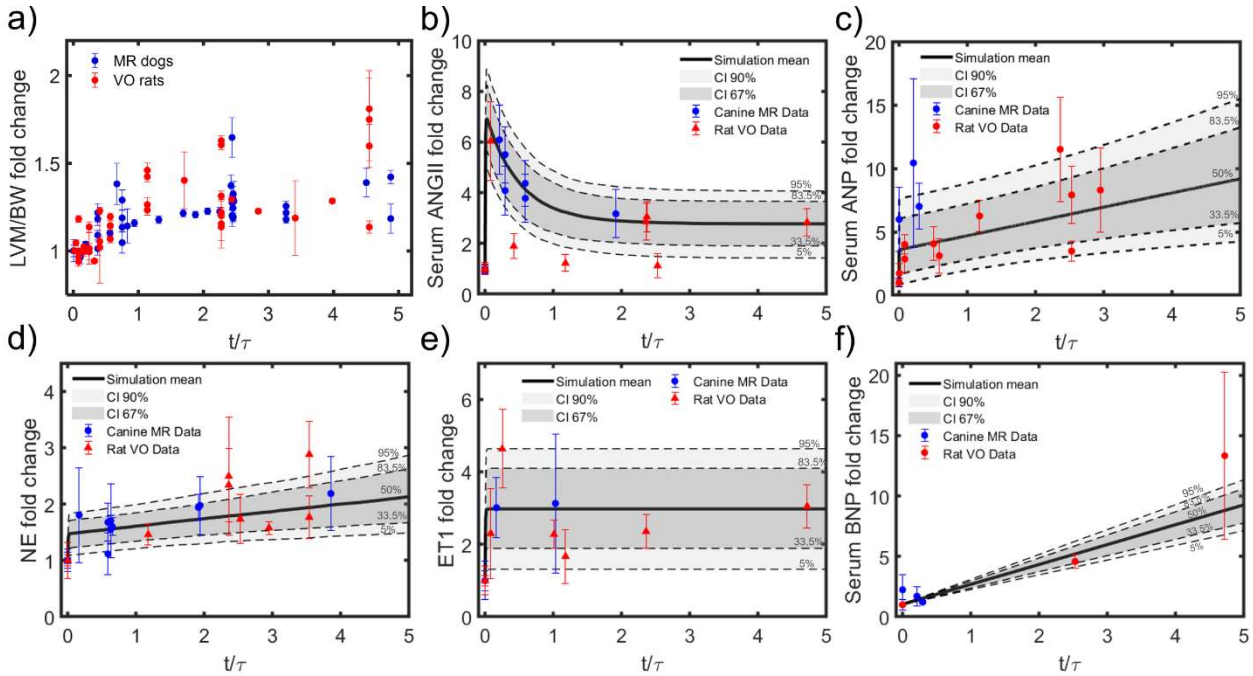

Fig 1. Integration of experimental data of MR in dogs and VO in rats. a) Fold changes in LVM/BW over time normalized to each species characteristic growth-time constant. Data-informed time-varying probability distributions of fold changes in circulating concentration of b) angiotensin II (ANGII), c) atrial natriuretic peptide (ANP), d) norepinephrine (NE), e) endothelin 1 (ET1), and f) brain natriuretic peptide (BNP). References for all experimental datapoints summarized in supplementary table S1.1 and fitted equations in table S1.3.

218 2.3. Time-varying hormonal input curves

219 We found baselines or control values of relevant hormone concentrations in blood were
220 consistent across animal sizes and species, suggesting a common homeostatic range
221 of circulating concentrations for each hormone. In this work, we assume that fold-
222 changes in concentration levels of those circulating hormones represented the intensity
223 of the neurohormonal response and would trigger proportional changes in the hormone-
224 receptor reaction input in the cardiomyocyte signaling model. The time resolved data of
225 serum concentrations were normalized to their corresponding baseline or control
226 concentration and plotted as a function of characteristic growth time (t/τ). We confirmed
227 that data from both species followed similar trends and fitted the integrated
228 experimental data with the simplest function that captured the temporal trends (Fig 1).
229 Details of the fitting process and the specific function fitted input dataset curved are
230 provided in the supplementary material section S1.2. and table S1.3 respectively.

231 2.4. Time-varying strain input curves

232 We assumed that changes in tissue-scale mechanical strain are proportionally
233 transduced to changes in the stretch input of the cardiomyocyte signaling model. Unlike
234 hormone concentrations, myocardial strain is a relative measure whose evolution over
235 time cannot be directly calculated from most published studies, so we must rely on a
236 mechanical model of the ventricular chambers to estimate strain from published
237 measurements. For the estimation of myofiber stretch, we assume the left ventricle to
238 be a thin-walled sphere. This oversimplification is not appropriate for some purposes
239 such as computing wall stress, but spherical models do capture the relation between
240 end diastolic volume and sarcomere length (Fig 2) [21], as well as the most salient

features of left ventricle pressure-volume behavior [22], and form the core of successful published phenomenological models of ventricular hypertrophy [23]. Consistent with most studies of low-pressure VO, we also assume pure eccentric hypertrophy, that is, all mass increments are deposited in the fiber direction while neglecting the thinning of the LV walls reported in some studies [24–26].

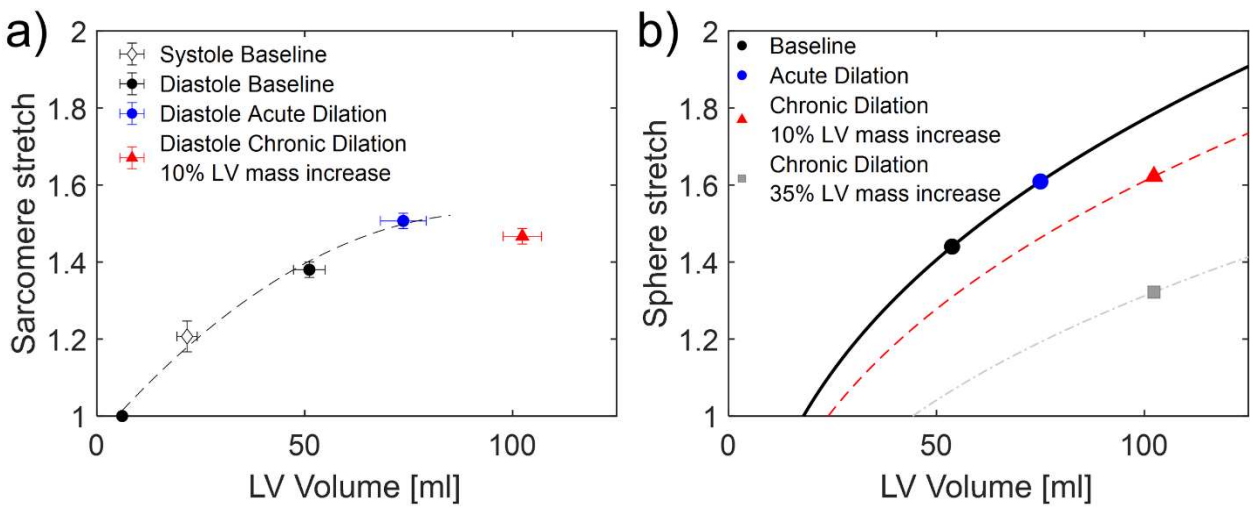

Fig 2. Spherical ventricular model correspondence to cardiomyocyte mechanics. a) Experimental measurements of sarcomere stretch in dog hearts under physiological loading conditions, in acute volume overload (Acute dilation) and long-term volume overload after 10% LV mass growth. Figure adapted from Ross et al. (1971) [21]. b) Replication of baseline, acute VO, and long-term VO conditions at diastole with a spherical ventricle model. The spherical model displays reasonable correspondence to experimental measurements at cellular scale. Notably, for a given amount of ventricle volumetric dilation an exacerbated increase in ventricular mass may bring sphere stretch below the baseline.

With these assumptions, the myofiber strain can be estimated at any time (t^i) as:

$$\varepsilon_{ED}^i = \frac{1}{2}\left[\left(\frac{V_{ED}^i}{V_0^i}\right)^{2/3} - 1\right], \qquad (1)$$

where V_{ED}^i is the end-diastolic volume at a given time, and V_0^i is the hypothetical unloaded (zero-pressure) volume. While the end-diastolic volumes V_{ED}^i are reported in the studies reviewed here or can be calculated from reported dimensions, changes in V_0^i must be estimated from reported changes in LV mass (Supplementary material S1.3).

The unloaded volume prior to the onset of overload (V_0^0) was estimated based on previous calculations of in vivo end diastolic stretch (λ_{ED}^0) [27], as well as zero-pressure ventricular volumes reported from experiments on healthy dogs [28]. A detailed derivation of strain probability distribution functions from experimental data is provided in Supplementary material S1.3.

Once calculated, strain was mapped to the network input myoStrain with an exponential function:

$$w_{myoStrain} = C_{myoStrain}(e^{D_{myoStrain}\,\varepsilon_{ED}} - 1) \quad (2)$$

2.5. Model of cardiomyocyte hypertrophic signaling pathways

We employed a published computational model of the hypertrophy signaling network that integrates many established pathways implicated in cardiac myocyte growth. The model consists of a logic-based network where the activity of each node follows a normalized Hill equation with possible activity values ranging from 0 and 1 [20,29]. The network consists of 106 nodes representing hormones and intracellular molecules and 192 reactions. The model has been used previously in the study of ventricular hypertrophy and was recently optimized in the context of β adrenergic stimulation [30]. The set of network parameters is summarized in supplementary table S2. In supplementary figure S1.1 we show a representation of the network model highlighting the nodes with available experimental data.

The influence of a reaction on the downstream nodes is modulated by the weight parameter w, which was left at the default value for all nodes except the inputs for AngII, ANP/BNP, ET1, NE, and stretch. The characteristic time constant governing the speed of changes in node activity was chosen as 0.005τ, for all intracellular reactions

and 0.02τ for output nodes reflecting protein synthesis, where τ is the fitted time constant for the exponential rise in LV mass, as discussed above. The network model was solved with Netflux (https://github.com/saucermanlab/Netflux). More detail about the network model formulation and solution method can be found in [31].

2.6. Bayesian inference analysis of experimental data

All parameter estimations required in our data processing pipeline were performed within a Bayesian inference framework. The Bayesian inference tool utilized for this study was a standard Markov Chain Monte Carlo (MCMC) algorithm with Metropolis-Hasting selection criteria and Gibbs sampling to navigate the multiparametric space. Briefly, the algorithm iteratively solves a numerical model while randomly varying its input parameters over a predetermined probability distribution, known as the prior probability distribution function (prior PDF) of the parameter space. On each iteration, the likelihood of the model's outputs is evaluated against experimental data. If the likelihood of the outputs with the current parameter set is larger than the likelihood of the previous iteration, the parameter set is saved. If the outputs for the current parameter set are less likely, the decision on whether to save the current parameter set is made randomly. After sufficient iterations, the collection of saved parameter sets converges to a new probability distribution of the parameter space, or posterior PDF, which are associated with probability distributions for the model predictions [32,33]. In this study, each MCMC algorithm was applied in two stages, first assuming a uniform probability distribution of the parameters within their physiologically plausible limits for 10,000 iterations. The resulting posterior PDF was then used as the prior PDF for a second run of the MCMC algorithm for additional 20,000 iterations, with a check to

verify the convergence of the solutions every 5,000 iterations (Supplementary material S1.4). The MCMC algorithm was programmed in MATLAB calling on Netflux. The source code including the transcript of experimental data is available at https://github.com/cardiacbiomechanicsgroup/MCMC_cardiomyocyte_VO_growth .

2.6.1. Probability distribution of hypertrophy network input weights

The normalized time-varying curves of hormone concentrations and mechanical strain provide information on how these stimuli vary over time but does not resolve their relative influence on cardiomyocyte function. One advance of the current work over previous applications of this network model is that we allow the key hypertrophic stimuli to have different weights. In the cardiomyocyte signaling network model, the weight of the hormone-receptor reaction determines its relative influence on the network for a given fold change in that hormonal input. The time-varying influence of a given input is calculated as the product of its baseline weight $\left(w^0_{species}\right)$ and its normalized time-varying fold-change curve (sections 2.3 and 2.4), where $w^0_{species}$ is unknown. We employed an MCMC to estimate the PDF of the baseline weights of hormone-receptor input reactions as follows. We first assumed a uniform prior PDF for the input weights of ANGII $\left(w^0_{AngII}\right)$, NE (w^0_{NE}), and ET1 (w^0_{ET1}) reactions. Sampling was constrained within the range for which the Cell Area output is sensitive to those inputs. Specifically,

$$\begin{aligned} 0.01 < w^0_{ANGII} < 0.15 \\ 0.01 < w^0_{NE} < 0.24 \\ 0.01 < w^0_{ET1} < 0.17 \end{aligned} \qquad (3)$$

For the rest of the hormone input reactions, we assign a single “background” reaction weight, sampled within the $0.01 < w_{background} < 0.4$ range. A preliminary study revealed

326 that, within the range of interest, the input reaction weights of ANP and BNP to
327 Guanylate Cyclase A (GCA) receptors have only marginal effects on predicted changes
328 in Cell Area; we therefore prescribed ANP/BNP the same weight as the background
329 species. We assigned null weight to the synthetic drug phenylephrine and isoproterenol
330 (ISO) reactions except when simulating drug infusions. We fixed the weight of the
331 mechanical stimulus input $\left(w^0_{myoStrain}\right)$ at a single value for each MCMC run and
332 repeated the process for $w_{myoStrain}$ values of 0.02, 0.04 0.05 0.055, 0.06, 0.065, 0.07,
333 0.08, and 0.09. The MCMC also estimates the probability distribution for the tissue
334 strain-to-myoStrain mapping parameter $C_{myoStrain}$, while parameter $D_{myoStrain}$ is
335 calculated for each MCMC iterations with equation 2 and $w^0_{myoStrain}$ and ε^0_{ED}.
336 On each step of the MCMC, the algorithm randomly samples the w^0_{ANGII}, w^0_{NE}, w^0_{ET1},
337 $w_{background}$, $C_{myoStrain}$ parameter space and randomly selects time-varying curves for
338 each stimuli from their respective PDFs (Fig 1 and Fig 3c). The likelihood of the model
339 outputs was evaluated against the experimental data on FAK, Akt, ERK5, ERK12,
340 ELK1, cGMP, p38, and JNK activity and cardiomyocyte growth (CellArea) from dog and
341 rat experiments. We added a condition assigning larger likelihoods to parameter sets
342 that produce a baseline CellArea activity near 0.5, in the most responsive region of the
343 sigmoidal curve.
344 Long-term experiments agree that LV mass plateaus at a new level in chronic stages of
345 VO [34]. We therefore assumed that continued growth at late time points and negative
346 growth (reversal of hypertrophy) at any time point were very unlikely. After convergence
347 of the MCMC we filtered out these very unlikely solutions and recorded the posterior
348 PDFs of the activity of the network nodes of interest.

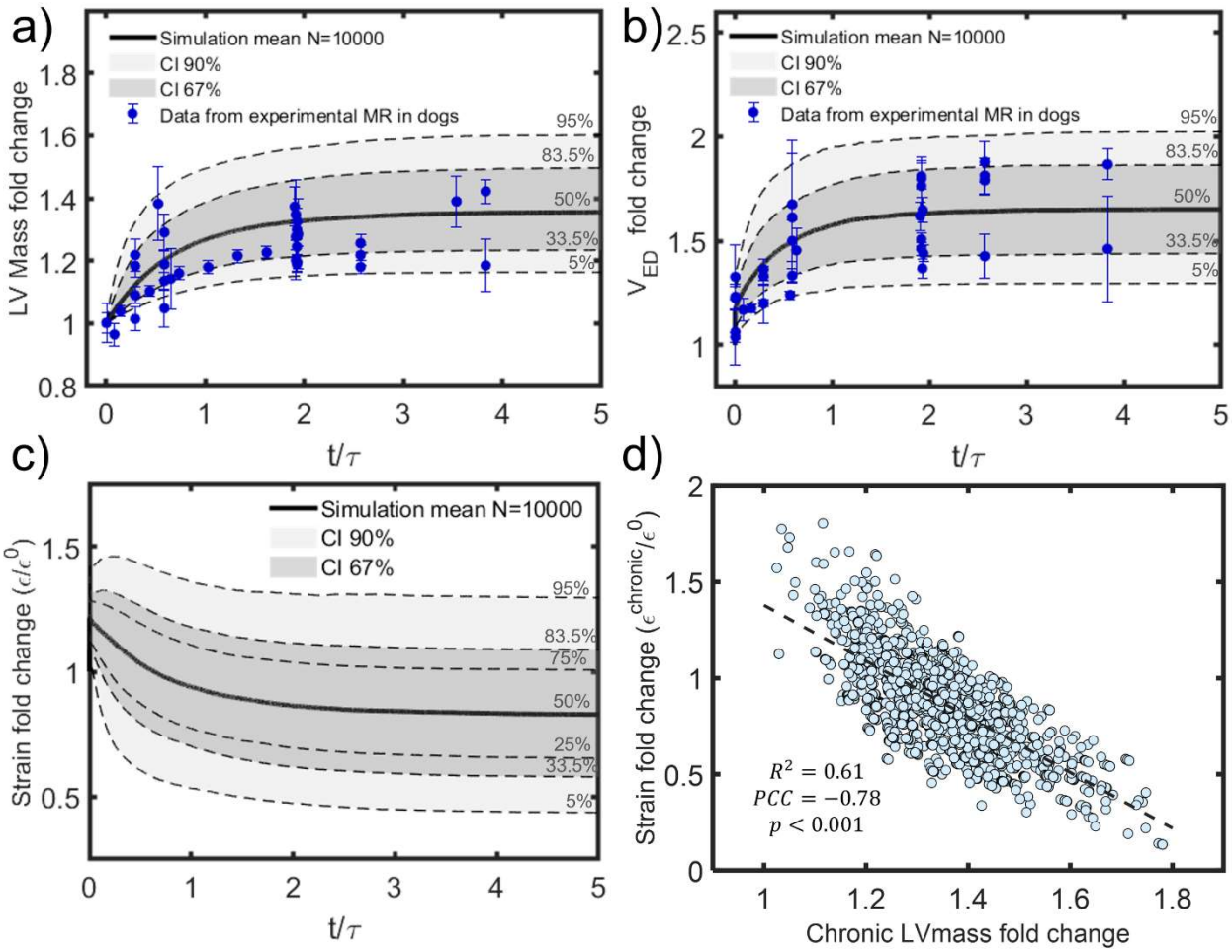

Fig 3. Results of the organ-scale data analysis. Time-varying probability distributions of a) LVM fold changes. b) End-diastolic volume (V_{ED}) fold changes, and c) Strain fold change. Influence of LVM and V_{ED} on the estimation of chronic fold changes in strain. LVM increment displays a strong inverse correlation with Strain changes. Sources for experimental measurements of LVM and V_{ED} are summarized in supplementary table S1.1.

2.7. Sensitivity analysis

We evaluated the sensitivity of network outputs (production of ANP, BNP, αMHC,βMHC, and SERCA) to the network inputs (weight of ANGII, NE, ET1, ANP and BNP to receptor reaction) by a standard correlation matrix based on statistical linear regression. The Pearson correlation coefficient (PCC) was calculated to quantify the parameter sensitivity. This method exploits the wealth of samples produced during the MCMC runs

362 to yield sensitivity estimates that are meaningful within the expected range of network
363 activity.

364 2.8. Validation of reaction weight posterior PDF

365 Data corresponding to the network outputs ANP, BNP, αMHC,βMHC, and SERCA were
366 not used in the estimation of parameter likelihoods during the MCMC runs. Thus, the
367 first round of validation consisted of comparing the estimated fold changes in activity
368 level of those output nodes to the corresponding fold changes in protein abundance
369 from experimental data.

370 We further validated the calibrated network model against data from independent
371 studies of *in vivo* drug stimulation of hypertrophy. For this, we performed *in silico*
372 replications of infusion experiments of ANGII in rats [35,36], NE in dogs [37–39], and
373 Isoproterenol (ISO) in mice [40] and compared the model-predicted changes in CellArea
374 to reported LV mass growth. We assumed that hormone infusion had no effects on
375 myoStrain.

376 The *in silico* replication consisted of increasing the input weight of the infused hormone
377 according to the circulating concentration fold-changes reported in experiments while
378 keeping the rest of the inputs at their baseline. Baseline values for the remaining inputs
379 were varied by sampling from their posterior PDFs over N=1000 iterations.

380 In the case of ISO infusion, a previous study by Estrada et al. determined that the
381 experimental dosages simulated here were sufficient to saturate the hypertrophic
382 response, so we imposed the maximum weight of 1 on the ISO node to simulate its
383 infusion.

384 2.9. Screening of pharmacological alternatives in the setting of VO.

We explored pharmacological alternatives for the treatment of hypertrophy in mitral regurgitation by using the calibrated and validated model to reproduce experimental VO conditions while knocking down the activity of key network nodes. First, we explored drug therapies conventionally used to treat heart failure: β-blockers, Angiotensin Receptor Blockers (ARB), and endothelin receptor antagonists (ET1A), independently and in paired combinations.

Next, we identified prospective non-conventional therapeutic targets by running a knock-down sensitivity analysis. For this we set the network model to its mean activity state for chronic VO, then ran iterative simulations in which we knocked down the activity of individual network nodes one by one and recorded the effect on the CellArea node. We calculated the knock-down sensitivity as $S_j = \left(\Delta y_{CellArea} / \Delta y_j \right) \left(y_j^0 / y_{CellArea^0} \right)$, where $\Delta y_{CellArea}$ and $y_{CellArea^0}$ are the change of activity and baseline activity of the CellArea node respectively, and Δy_j and y_j^0 are the change in activity baseline activity of the knocked-down species.

The effect of the drugs on VO-induced hypertrophy was assessed by running standard Monte Carlo simulations (N=1000) with random samples over the PDF of baseline reaction weights, and time-varying fold changes of hormone concentrations and strains characteristic of VO, while assigning null activity to network nodes corresponding to the drug action. Finally, we compared the predicted effect of conventional drugs on growth to the reports by Sabri et al. and Pat et al. on β-blockers [15,16] Murray et al. (2008,2009), Francis et al., and Lee et al. on ET1A [41–45] and Perry et al. and Zhang et al. on ARB [26,46] (Supplementary table S1.2).

3. Results

3.1. Probability distributions of fiber strain.

We produced a data-informed continuous probability distribution of end-diastolic strain (ε_{ED}) relative to an unloaded state over the course of experimental VO. The PDF display the expected trends over time, that is, an acute increase in strain owing to the sudden increase of V_{ED}, followed by a gradual decrease driven by the compensatory hypertrophic response (Fig 3). As V_{ED} and LVM curves reach a plateau in chronic VO stages, ε_{ED} also stabilizes at a magnitude close to its baseline. Models in which mechanical strain is the only promoter of cardiomyocyte growth only produce this stable hypertrophied state if strain returns to its baseline level, or the homeostatic strain level is allowed to adapt [13,47]. Interestingly, our data analysis suggests that in 75% of the cases, strain falls below its original baseline level in chronic stages of experimental VO (Fig 3c), with 50% of the cases passing below this threshold relatively early ($t/\tau \leq 1$ corresponding to the first 12 days in rats and 6 weeks in dogs). Myofiber strain showed a strong inverse correlation to LVM fold change (PCC=-0.78), suggesting that myofiber stretch falling below baseline is more likely to occur in cases with the greatest mass increase (Fig 3d).

3.2. Cross-species data integration and probability distribution of hormonal stimuli.

The best-fit characteristic time constant for mass growth is (τ_M) 1095 hours for dogs and 283 hours for rats. The ratio of the species time constant is $\tau_{M_{dog}}/\tau_{M_{rat}} = 3.86$. Interestingly, this ratio is close to the proportion between the heart rates (HR) of the sampled populations, which is often used for allometric scaling [48]. With an average HR of $363 \pm 14\ bpm$ for rats and $95 \pm 4\ bpm$ for dogs, the ratio is $HR_{rat}/HR_{dog} = 3.82 \pm 0.22$.

3.3. Probability distribution of input stimuli reaction weights

In this section we present the results of the Bayesian analysis of the signaling network model and probabilistic fitting of its input parameters. Preliminary screenings of the parameter space revealed that the baseline weight of the myoStrain input $\left(w^0_{myoStrain}\right)$ greatly modulated the occurrence of experimentally unlikely solutions, such as growth reversal and runaway growth that never stabilized. We therefore ran a series of MCMCs with fixed $w^0_{myoStrain}$ while randomly sampling the rest of the input reaction weights as described in section 2.6.1. We found that constraining the baseline weight of the myoStrain input within the range $0.055 \leq w^0_{myoStrain} \leq 0.060$ minimized the number of unlikely solutions. For $w^0_{myoStrain} > 0.06$, the solutions tend to be dominated by the myoStrain input, resulting in a reversal of growth at later time points despite continuing simulated overload, while the solutions for $w^0_{myoStrain} < 0.05$ were dominated by adrenergic stimulation, increasing the chances of runaway growth (Supplemental material S1.5). The results presented here were therefore obtained with a fixed $w^0_{myoStrain} = 0.06$, which was associated with the highest mean likelihood among the myoStrain values we tested.

The posterior PDF of the remaining input reaction weights converged to:

$$\begin{aligned} w_{ANGII} &= 0.010 \pm 0.002 \\ w_{NE} &= 0.033 \pm 0.014 \\ w_{ET1} &= 0.056 \pm 0.025 \\ w_{background} &= 0.031 \pm 0.022 \end{aligned} \tag{4}$$

448 We calculated correlations among these inputs weights. The strongest correlation was
449 between w_{ET1}^{0} and $w_{background}^{0}$ with a Pearson PCC=-0.42, while all other PCC
450 magnitudes were below 0.3.
451 The network outputs were insensitive to the strain-to-myoStrain mapping parameters.
452 The PDF of the mapping parameter converged to $C_{myoStrain} = 5.86 \pm 1.38$.

453 3.4. Sensitivity analysis

454 The sensitivity revealed that all network outputs were far more sensitive to ET-1 than to
455 any of the other network inputs examined in this study (Fig 4). This suggests that, in
456 chronic stages of VO, variation in ET-1 circulating concentrations within its probable
457 range has the largest influence on cardiomyocyte size and function of any individual
458 hormonal or mechanical growth factor. According to this analysis, higher levels of ET-1
459 in chronic stages of VO are associate with greater cardiomyocyte growth, greater
460 myocardial production of βMHC, ANP and BNP, and reduced myocyte synthesis of
461 SERCA and αMHC (Fig 4). This result is consistent with the knock-down sensitivity
462 analysis, where the elimination of ET-1 stimulation produced the largest change in
463 activity of multiple signaling nodes downstream of ET-1 including calcium, calmodulin
464 (CaM), CaM kinase, and mTor (Supplementary figures S1.10, S1.11). This result
465 implies that among the circulating hormones known to be altered during VO,
466 manipulating ET-1 levels, receptor-activity, or signaling should offer the greatest
467 potential to modulate hypertrophy and other myocardial responses to VO. This
468 hypothesis is explored further in Section 3.6 below.
469
470

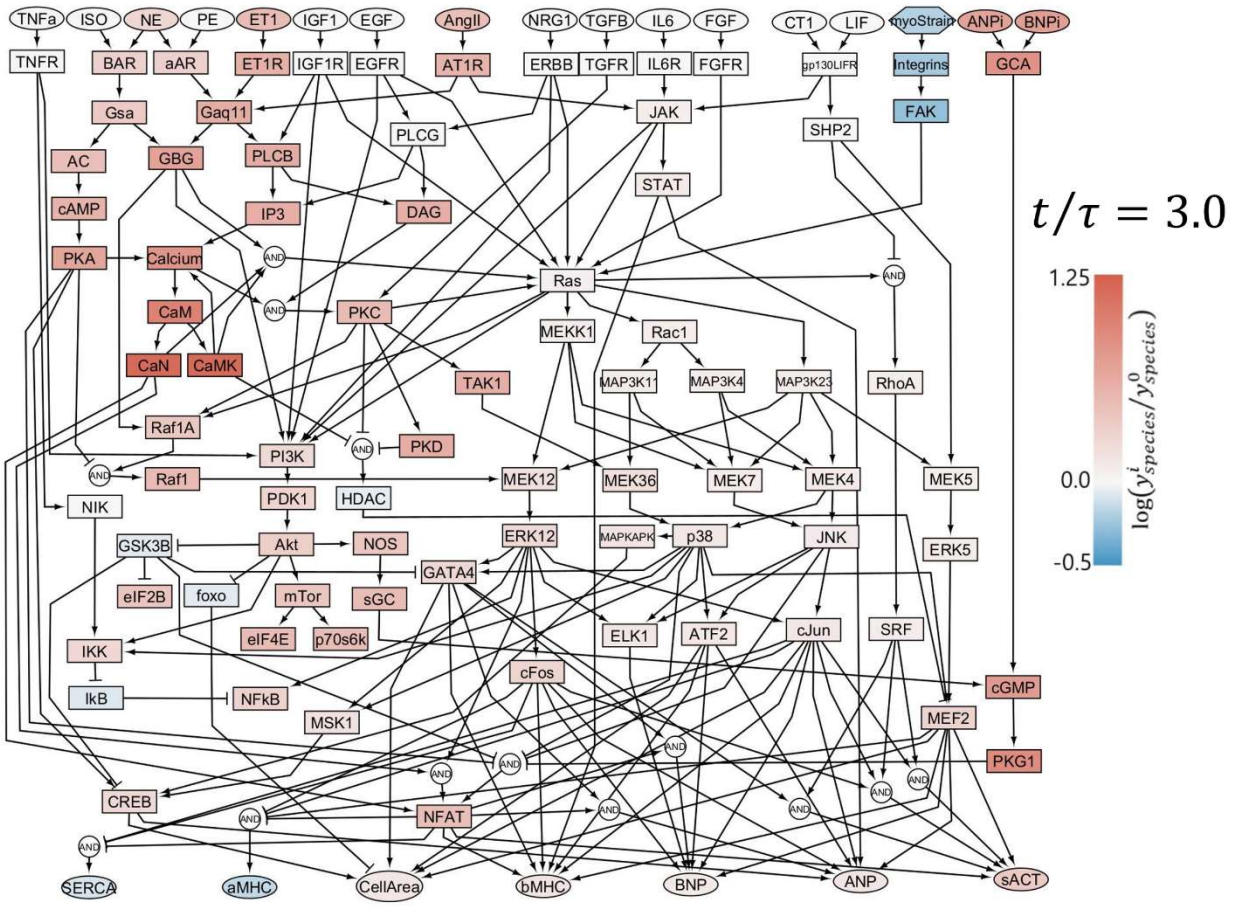

Fig 4. Sensitivity analysis of network outputs to inputs in chronic stages of chronic VO. Each marker represent the final state of a simulated VO experiment. A linear regression model (dashed line) is fit to each simulation-generated output-input pair. Pearson PCC is displayed on the upper left corner of each. The PCC represents the relative influence of inputs on each output, with ET1 displaying the largest influence on all outputs.

3.5. Validation

The calibrated model properly predicts the activation of the fetal gene program in the context of experimental volume overload, including the downregulation of SERCA and αMHC and upregulation of ANP, BNP, and βMHC (Fig 5).

The model predictions of myocyte protein synthesis also quantitatively agree with the magnitude of measured fold changes in SERCA, aMHC, and bMHC abundance in cardiac tissue, but underestimate the magnitude of observed changed in ANP and BNP

(Fig 6a). Notably, our model reproduces the reported dephosphorylation of FAK and decrease in Integrin activity during chronic volume overload (Supplementary figure S1.9) [15–17]. This finding was independent of the choice of strain-to-myoStrain mapping function. Rather, because integrins and FAK are directly downstream of myoStrain in the network model, this result was a direct consequence of the data-driven prediction that tissue-scale strain falls below its baseline in most cases of experimental volume overload (Fig 5).

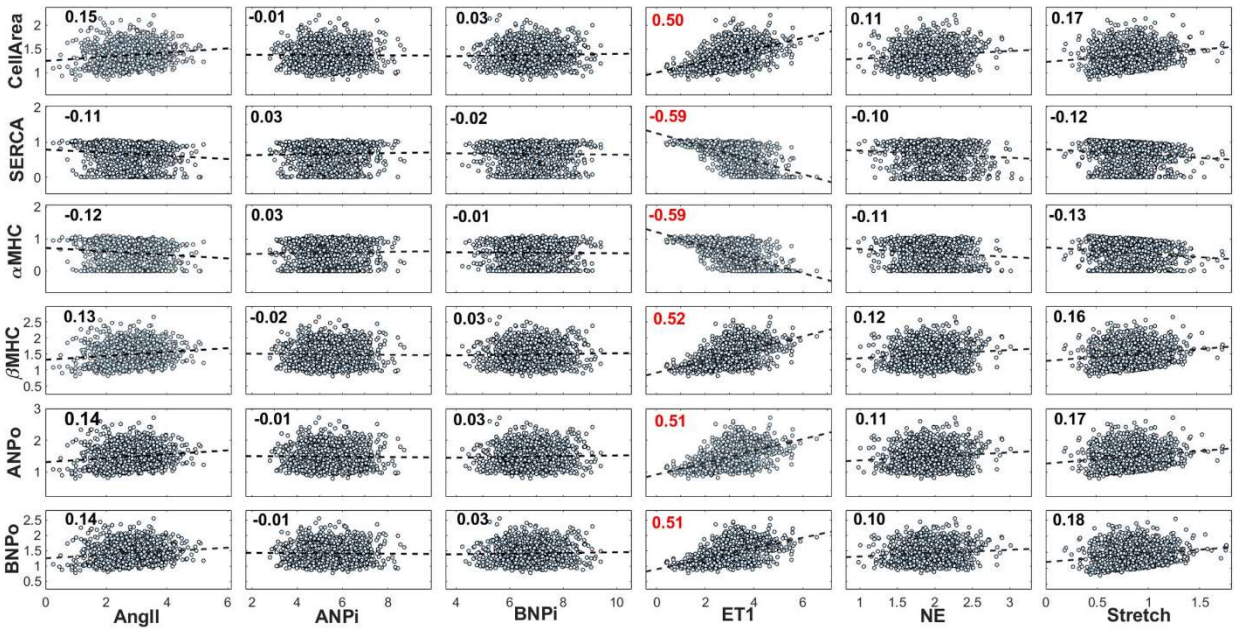

Fig 5. Diagram of cardiomyocyte signaling network model. The color-code indicates the logarithm of the fold change in activity of each node in chronic stages of VO respect to baseline, red means protein activity/abundance is above baseline and blue indicates protein activity/abundance falls below baseline.

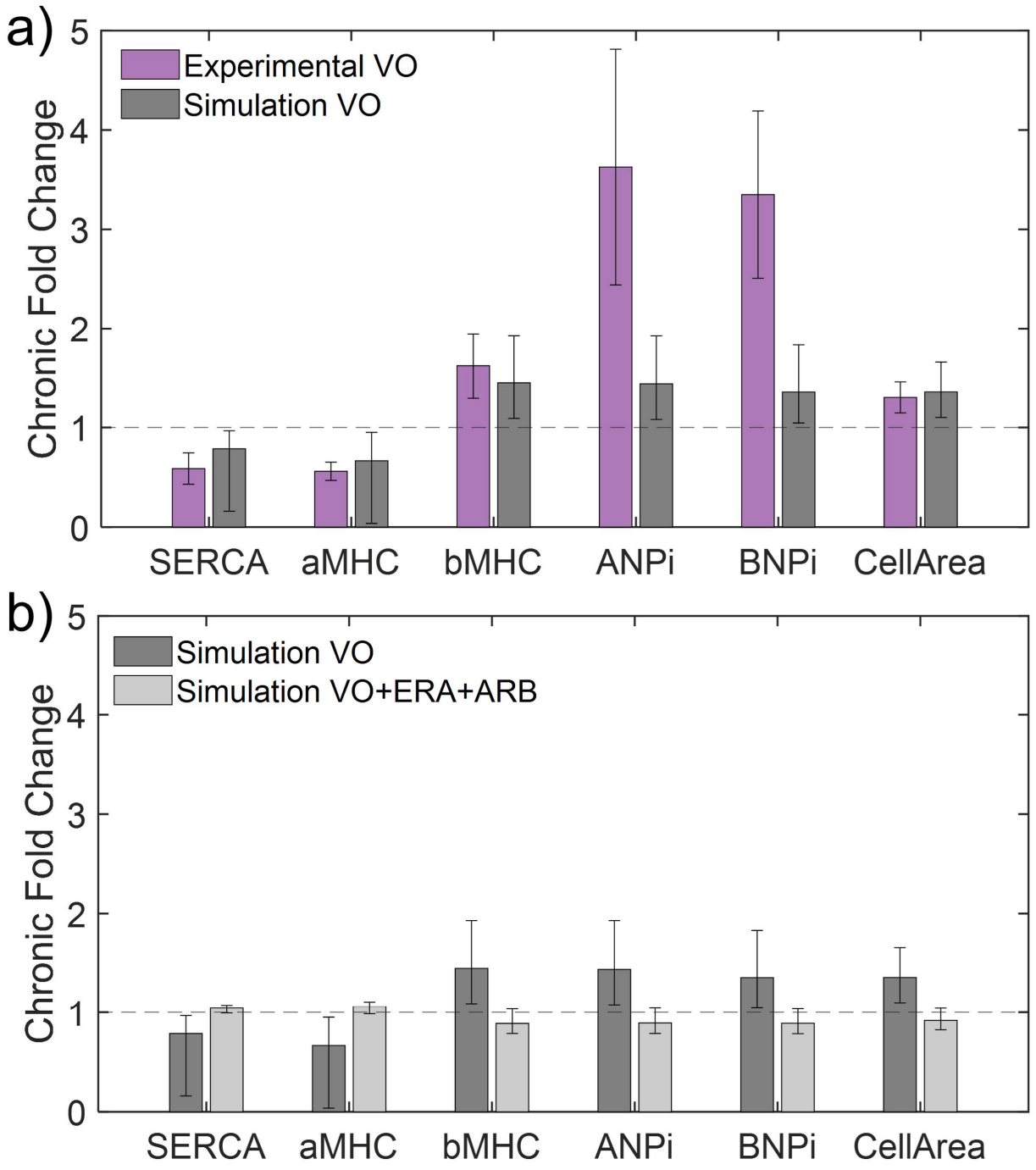

Fig 6. Activity of network output nodes as representation of cardiomyocyte function. a) Validation of calibrated model predictions of network output nodes representing protein abundance of SERCA (Zheng et al. 2009) [17], aMHC, bMHC (Freire et al. 2007, Lachance et al. 2014) [49,50], ANP (Fareh et al. 1996) [51], BNP (Zheng et al. 2009, Fareh et al. 1996) and growth Cell Area (Urabe et al. 1992) [17,51,52]. The model (gray bars) shows good agreement with the trends observed from in vivo experiments in dogs and rats (purple bars). b) Effect of ERA+ARB treatment in the context of VO. The model predicts the combination of endothelin receptor antagonists (ERA) and angiotensin receptor blockers (ARB) has the potential to revert cardiac hypertrophy and inactivate the fetal gene program (light gray bars).

Next, we simulated published studies of chronic infusion of individual hormones that play a role in volume-overload-induced growth. Sustaining elevated NE circulating concentration 15.4 ± 1.9 fold times above normal levels for one month $(t/\tau = 0.7)$ produced a simulated growth of $26 \pm 9\%$, which is reasonably close to the reported $20 \pm 5\%$ by King et al. [38]. Sustaining a circulating NE concentration 7.4 ± 0.9 fold times above normal levels for 3 months $(t/\tau = 2.0.)$ produced a simulated growth of $33 \pm 17\%$, which was larger than the reported increase in LV mass of $15 \pm 6\%$ (Fig 7a). It is important to highlight that these two studies evaluated both different concentrations of NE and different time periods of infusion.

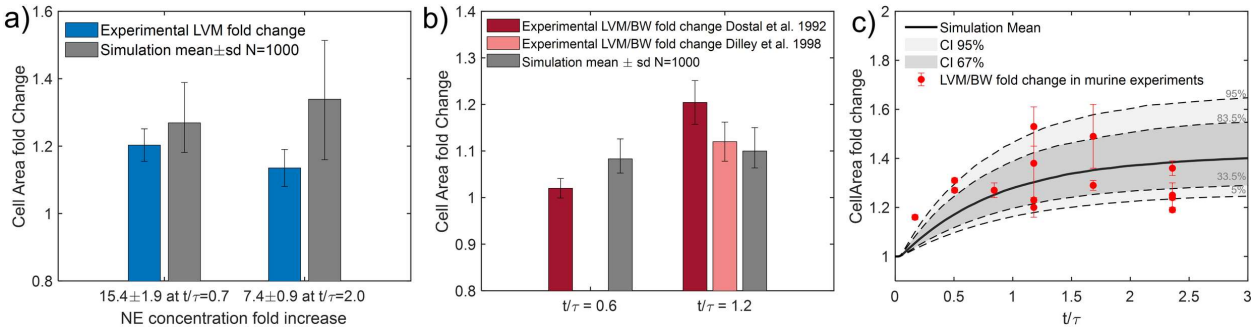

Fig 7. Validation of model predictions on the effect of growth factor infusions against experimental data. a) Prediction of growth (gray bars) by infusion of NE against experiments in dogs by King et al. (1987) (left blue bar) [38], and Laks et al (1973) (right blue bar) [37]. b) Prediction of growth (gray bars) by ANGII infusion against experimental data by Dostal et al. (1992) (dark red bars) and Dilley et al. (1998) (light red bars) [35,36]. c) Time-varying probability distribution of growth by infusion of isoproterenol against experimental data in mice (red markers), as compiled by Estrada et al. (2020) [40].

When we reproduced the ANGII infusion experiments by Dilley et al. and Griffin et al. by imposing a fold-change increase in ANGII of 3.5 ± 0.3, the predicted cardiomyocyte growth of $11 \pm 4\%$ agreed well with reported ventricular mass growth in both experiments (Fig 7b). Simulating a saturating dose of ISO infusion in mice also

530 produced a cardiac growth curve that matched published data well, when the
531 characteristic growth time was scaled using the mice-to-dog heart rate ratio (Fig 7c).

532 3.6. Screening of pharmacological alternatives for treatment of VO.

533 To explore possible therapeutic alternatives for the treatment of mitral regurgitation, we
534 simulated the effect of several interventions related to circulating hormones elevated
535 during VO. We simulated the effects of endothelin receptor blockers (ERA), angiotensin
536 receptor blockers (ARB), and β-blockers, administered throughout the course of VO
537 independently and in paired combinations. The largest mean effect of a single drug was
538 produced by ERA, which reduced CellArea growth from $35 \pm 24\%$ to only $6.5 \pm 11\%$, an
539 effect that is supported by empirical evidence (Fig 8a). In rat VO experiments, ERA
540 significantly reduced the LVM/BW ratio and reduced ventricular remodeling with respect
541 to controls [41–44,53]. By contrast, our model predicted that total blockade of the AT1
542 receptor would result in a $-10 \pm 40\%$ reduction in CellArea growth relative to untreated
543 controls, an effect that should be statistically undetectable given the high variability (Fig
544 8b). This result also agreed with negative results by Perry et al. and Dell'Italia et al. in
545 dogs and by Zhang et al. in rats, who reported that neither ARB nor angiotensin
546 converting enzyme inhibitors (ACEi) improved left ventricular function or significantly
547 reduced hypertrophy in experimental MR in dogs [26,46,54]. In dogs, β-blockers do not
548 produce any effect on ventricular mass in the first month of VO $(t/\tau < 0.7)$ [55], but
549 chronic use of this drug $(t/\tau > 2.7)$ appears to exacerbate hypertrophy in dog and rat
550 models of VO [14,16]. In our model, β-blockers produced a negligible mean effect
551 across all stages of VO (Fig 8c).
552

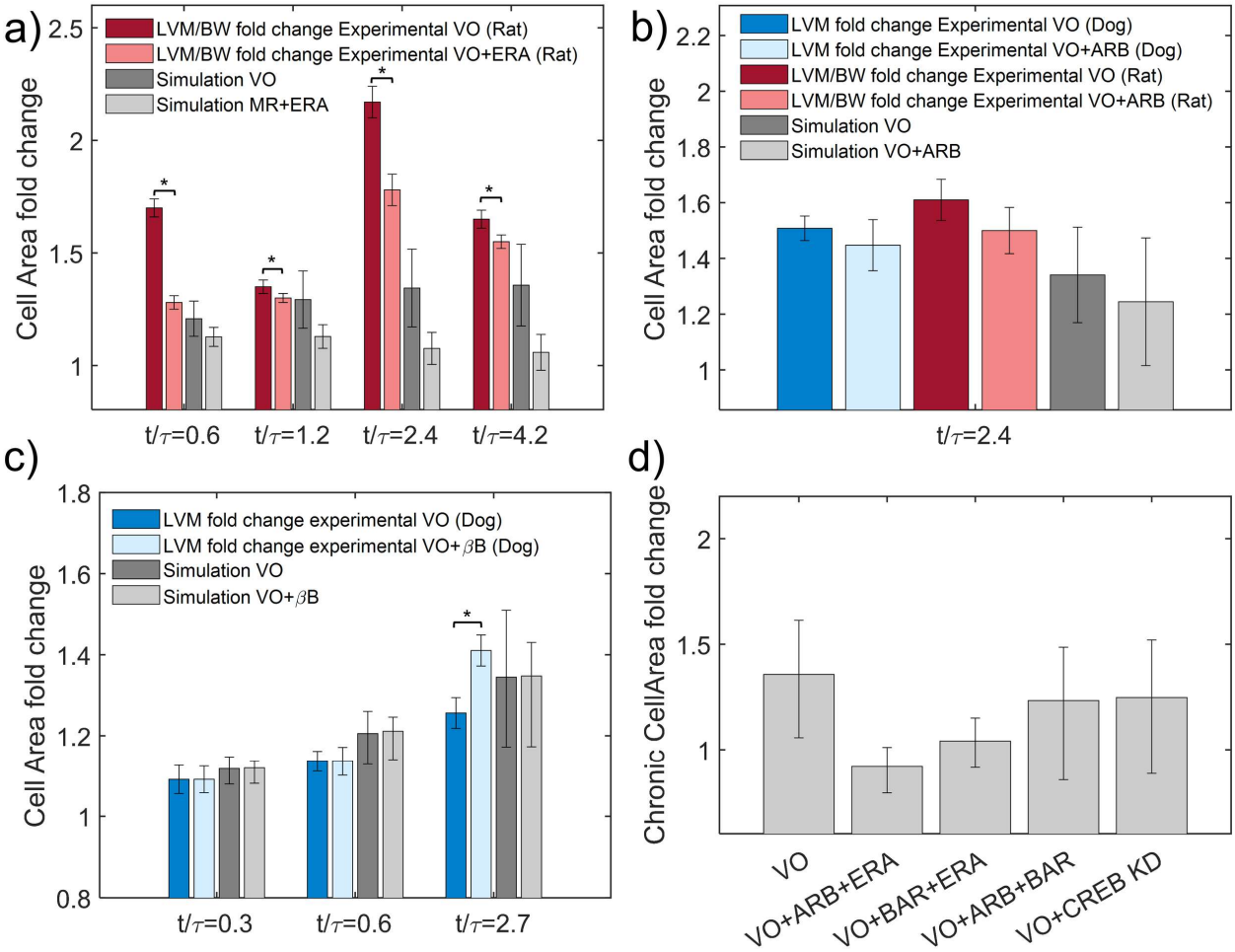

Fig 8. Model predictions on the effect of drug treatments in the context of VO. a) Predictions on the effect of endothelin receptor antagonist (ERA) on mass growth in VO (gray bars), and validation against experimental data on ERA treatment of VO in rats (red bars) by Francis et al. 2004 $(t/\tau = 0.6)$, Murray et al. 2008 $(t/\tau = 1.2)$, Lee et al. 2005 $(t/\tau = 2.4)$, and Murray et al. 2009 $(t/\tau = 4.2)$ [41–43,45]. b) Predictions on the effect of angiotensin II recepot blockers (ARB) on mass growth in VO (gray bars), and validation against experimental data on ARB treatment of VO in rats (red bars) by Zhang et al. 2010 [26,46], and in dogs (blue bars) by Perry et al. 2002 at $t/\tau = 2.4$. c) Predictions on the effect of β-blockers on mass growth in VO (gray bars), and validation against experimental data from dog models (blue bars) by Sabri et al. 2008 $(t/\tau \leq 0.6)$ and Pat et al. 2008 $(t/\tau = 2.7)$ [15,16]. d) Prediction on the effect of combined drug therapies and CREB knock down in chronic VO $(t/\tau = 3.0)$ (light gray bars). ERA combinations, particularly ERA+ARB show largest potential to revert cardiac hypertrophy in VO. The * symbol indicates t-test statistical significance p<0.05.

When simulating pairwise combinations of these drugs, ERA plus ARB (ERA+ARB) produced the largest predicted effect on ventricular hypertrophy, returning CellArea to its original size and deactivating the fetal gene program (Fig 6b, 8d). In line with this

prediction, Leskinen et al. report the combination ERA+ARB blocked natriuretic peptide synthesis by the cardiac tissue [56].

When we knocked down intermediate nodes individually in the context of simulated volume overload. Only CREB knock-down produced a mean CellArea decrease larger than 10%, with a total effect $-11 \pm 42\%$. However, the large variability suggests even this effect would be undetectable in practice (Fig 8d). In the supplementary material section S1.6. we compare how CREB knock-down performs against the blockade of hormonal and mechanical stimuli, producing a similar mean effect on CellArea as ARB. However, as CREB is located downstream the signaling reaction cascade, it has no effects on intermediate signaling proteins (Supplementary figures S1.10, S1.12).

4. Discussion

This study used a Bayesian approach and well-established models of cardiac hypertrophy to integrate a large body of experimental VO data in rats and dogs. The resulting model can produce probabilistic predictions of cardiomyocyte hypertrophic response to neurohormonal and mechanical stimulation, with an appropriate propagation of experimental and model-induced uncertainty into the model's outputs. The calibration against the activity of multiple signaling proteins in independent and interconnected pathways enabled the adjustment of the relative influence of each growth stimulus. The calibration was reasonably successful when tested against NE, ISO, and ANGII infusions and the effect of various receptor blockers administered during experimental VO.

The model identifies ET1 as one of the main drivers of hypertrophy in chronic stages of VO. Consequently, the model predicts that the most effective strategies to block VO-

594 induced hypertrophy are combination therapies with multiple blockers including ERA,
595 especially with ARB, which mostly returns cardiomyocyte size to normal and deactivates
596 the fetal gene program.

597 The study of Leskinsen et al. 1997 and Fareh et al. 1996 on ERA+ARB effects on
598 neurohormonal profiling in VO in rats showed that the combined inhibition of both
599 receptors blocked the cardiac natriuretic peptide synthesis and reduced intracellular
600 Calcium concentration. The authors suggest that hormonal stimulation mostly regulates
601 cardiac secretion with myocyte stretch having marginal influence. The authors also
602 suggest that ET1 stimulation is more important in regulating the myocyte adaptative
603 response to VO than AngII [51,56]. Both observations confirm some of the most
604 prominent model predictions. Furthermore, according to several studies, ERA treatment
605 prevents cardiac growth and remodeling and cytokine expression in rat models of VO
606 [41–45]. Despite the apparent benefits of ERA in experimental VO and its proven
607 vasodilator effect, their clinical use has been limited by potentially severe side effects,
608 such as alterations of liver function, anemia, and edema. The most common clinical
609 application of ERA is to treat pulmonary artery hypertension, and recent efforts point to
610 the development of selective ERAs for treating persistent hypertension [57].

611 Our model suggests that the effect of NE as a growth factor is marginal in experimental
612 VO. The exaggerated NE concentration levels required by Laks et al. and King et al. to
613 produce LV mass increases below 20% support this notion [37,38]. In consequence, our
614 model predicts only negligible effects of β-blockade on cardiac hypertrophy at any stage
615 of VO. This prediction agrees well with observations in isolated cardiomyocytes, and
616 short-term experiments in vivo. However, chronic β-blockade during experimental VO

617 appears to exacerbate hypertrophy after several months in dogs [16,58,59]. We
618 hypothesize that this observation results from an indirect of β-blockade on hypertrophy
619 through modulating of LV contractility, an effect that is not included in the model
620 employed here. Evidence supporting that hypothesis includes the fact that β-blockade
621 partially restores FAK phosphorylation levels during experimental VO, indicating
622 increased activation of stretch-modulated hypertrophic pathways [14–16,60].

623 In clinical studies, β-blockers improves LV function, symptoms, and survival in patients
624 with chronic MR and heart failure (A. Ahmed & Dell'Italia, 2004; M. I. Ahmed et al.,
625 2012), but these benefits appear to be due to modulation of changes in signaling
626 pathways that occur with heart failure, effects not modeled in the present study.

627 One of the most interesting implications of our analysis is our prediction that in most
628 cases of VO, the combination of early overstretch and sustained neurohormonal
629 activation trigger sufficient hypertrophy to drive stretch below its baseline levels. This
630 prediction did not derive from the signaling network but rather from the Bayesian
631 approach to integrating published data on observed LV mass and volume increases
632 across a large number of experimental studies (Fig 2b,3c). This prediction may explain
633 the otherwise puzzling depression in the activity of key mechano-transduction proteins
634 in the context of volume overload. While FAK phosphorylation is elevated in pressure
635 overload and aortic valve regurgitation relative to baseline, FAK phosphorylation is
636 reduced in VO despite elevated LV volumes that are commonly assumed to indicate
637 elevated levels of myocyte stretch [15,16]. Interestingly, experiments on skeletal muscle
638 demonstrate that FAK dephosphorylation is a marker of mechanical unloading [61,62],
639 and the genetic restriction of FAK activity induces dilated thin-wall LV cardiomyopathy in

640 mice when challenged with pressure overload [63], evidence that stablishes an
641 interesting link between the dilated ventricle phenotype and mechano-transduction
642 depression. In previous work, we identified Ras as a relevant hub responsible for the
643 crosstalk of multiple pathways [20,29]. In the current work we found Ras was a critical
644 node integrating the competing effects of mechanical stretch and neurohormonal inputs
645 in VO. During early VO, elevated stretch and neurohormonal stimulation drove strong
646 activation of Ras, while in chronic VO reduced stretch was offset by continuing
647 neurohormonal stimulation, maintaining a low level of Ras activation (Fig 5,
648 Supplementary material 3).

649 **5. Limitations and future directions**

650 The ability to predict not only mean responses but also the uncertainty around those
651 predictions is a major advantage of Bayesian approaches. However, one important
652 limitation of the analysis presented here is that the range of uncertainty in our model
653 predictions is noticeably wider than the uncertainty in the experimental data used for
654 validation. Part of this predicted uncertainty is the inevitable consequence of integrating
655 disparate sources of data, which included the work of several research groups on
656 animals of different sizes and species and applying two different models of VO. Another
657 likely contributor is that we treated the levels of the various circulating hormones as
658 independent of each other; for example, some of our randomly selected parameter sets
659 will include extreme increases of AngII and low levels for the rest of the hormones.
660 However, in reality most reports suggest that the expression of these neurohormones is
661 correlated to the severity of cardiac insult, and therefore to each other. The current
662 model also lacks output-to-input feedback loops. For example, the strain-time curve is

663 imposed through random sampling, with no previous knowledge of the growth response,
664 and the CellArea likelihood is evaluated all available data on mass increases, not just
665 those occurring at a similar level of strain. Another limitation worth mentioning is that the
666 current model ignores the mechanical effects of neurohormonal alterations. Notably, the
667 drugs tested herein are known to have vasodilating effects, while AngII is a potent
668 vasoconstrictor, so changes in their concentrations modulate ventricular afterload. The
669 activity of adrenergic receptors modulates the muscular tone and contractile function of
670 the heart, thus potentially also modulating the mechanical strain. To address these
671 sources of variability, we can introduce additional experimental data and covariance
672 relations to the likelihood evaluation and incorporate this model of isolated
673 cardiomyocytes into a multiscale model of cardiovascular function. A multiscale model
674 could couple the amount of predicted cardiomyocyte growth to tissue and organ-scale
675 ventricular models to update the estimations of myocardial strain and introduce
676 feedback loops between systemic hemodynamics, neurohormonal alterations, drug
677 effects, and heart loading. One of the advantages of the Bayesian inference approach is
678 that all these proposed model improvements and data additions can be built on top of
679 the present work to narrow the range of predicted uncertainty.

680 We assumed changes in neurohormonal circulating concentrations are proportionally
681 transduced into receptor activity; this assumes large receptor availability and non-
682 competitive binding, neglects changes in receptor abundance, and ignores possible
683 differences in hormonal concentrations between the bloodstream and the immediate
684 cellular environment. Hormone concentrations in myocardial tissue extractions can be
685 several orders of magnitude larger than circulating concentration. However, they

686 showed similar trends, suggesting that the circulating and local values are at least
687 correlated (Dell'Italia et al., 1995, 1997; Tallaj et al., 2003). Ultimately, calibrating the
688 model to widely accessible data such as serum concentrations improves its translational
689 value.

690 ## 6. Conclusions

691 We present a comprehensive data analysis of experimental data of volume overload
692 using a cardiomyocyte signaling model within a Bayesian inference framework. The
693 calibrated model suggests that growth in experimental VO is mostly driven by the
694 neurohormonal response, with the myocardial tissue stretch being compensated in early
695 stages of VO. The model suggests that Endothelin1 receptor activity plays a central role
696 in driving hypertrophic responses and the activation of the fetal gene program. The
697 model predicts the combination of ERA and ARB as a potential therapeutic alternative
698 to dampen cardiomyocyte hypertrophy and dysfunction in VO. Our model provides a
699 plausible explanation for the depression of mechano-transduction signaling pathway in
700 experimental VO, despite the widespread conception of volume overload hypertrophy
701 as driven by myocyte overstretch.

702 ## 7. Acknowledgements

703 The authors thank Dr. Pim Oomen, University of California Irvine, for his support and
704 guidance on the selection and development of the Bayesian analysis method.

705 ## 8. References

706 [1] Wu S, Chai A, Arimie S, Mehra A, Clavijo L, Matthews R V., et al. Incidence and treatment of
707 severe primary mitral regurgitation in contemporary clinical practice. Cardiovascular
708 Revascularization Medicine 2018;19:960–3. https://doi.org/10.1016/J.CARREV.2018.07.021.

[2] Carabello BA. The Current Therapy for Mitral Regurgitation. J Am Coll Cardiol 2008;52:319–26. https://doi.org/10.1016/J.JACC.2008.02.084.

[3] Lorell BH, Carabello BA. Left Ventricular Hypertrophy. Circulation 2000;102:470–9. https://doi.org/10.1161/01.CIR.102.4.470.

[4] Oyama MA. Neurohormonal activation in canine degenerative mitral valve disease: implications on pathophysiology and treatment. Journal of Small Animal Practice 2009;50:3–11. https://doi.org/10.1111/J.1748-5827.2009.00801.X.

[5] Komajda M, Pousset F, Isnard R, Lechat P. The role of the neurohormonal system in heart failure. Heart 1998;79:S17. https://doi.org/10.1136/HRT.79.2008.17S.

[6] Le Tourneau T, De Groote P, Millaire A, Foucher C, Savoye C, Pigny P, et al. Effect of mitral valve surgery on exercise capacity, ventricular ejection fraction and neurohormonal activation in patients with severe mitral regurgitation. J Am Coll Cardiol 2000;36:2263–9. https://doi.org/10.1016/S0735-1097(00)01015-9.

[7] Chen HH, Schrier RW. Pathophysiology of Volume Overload in Acute Heart Failure Syndromes. Am J Med 2006;119:S11–6. https://doi.org/10.1016/J.AMJMED.2006.09.012.

[8] Wilson K, Lucchesi PA. Myofilament dysfunction as an emerging mechanism of volume overload heart failure. Pflugers Arch 2014;466:1065–77. https://doi.org/10.1007/s00424-014-1455-9.

[9] El Sabbagh A, Reddy YNV, Nishimura RA. Mitral Valve Regurgitation in the Contemporary Era: Insights Into Diagnosis, Management, and Future Directions. JACC Cardiovasc Imaging 2018;11:628–43. https://doi.org/10.1016/J.JCMG.2018.01.009.

[10] Zheng J, Li Y, Billor N, Ahmed MI, Fang Y-HD, Pat B, et al. Understanding post-surgical decline in left ventricular function in primary mitral regurgitation using regression and machine learning models. Front Cardiovasc Med 2023;10. https://doi.org/10.3389/fcvm.2023.1112797.

[11] Otto CM, Nishimura RA, Bonow RO, Carabello BA, Erwin JP, Gentile F, et al. 2020 ACC/AHA Guideline for the Management of Patients With Valvular Heart Disease: A Report of the American College of Cardiology/American Heart Association Joint Committee on Clinical Practice Guidelines. Circulation 2021;143:E72–227. https://doi.org/10.1161/CIR.0000000000000923.

[12] Kerckhoffs RCP, Omens JH, McCulloch AD. A single strain-based growth law predicts concentric and eccentric cardiac growth during pressure and volume overload. Mech Res Commun 2012;42:40–50. https://doi.org/10.1016/j.mechrescom.2011.11.004.

[13] Witzenburg CM, Holmes JW. A Comparison of Phenomenologic Growth Laws for Myocardial Hypertrophy. J Elast 2017;129:257–81. https://doi.org/10.1007/s10659-017-9631-8.

[14] Seqqat R, Guo X, Rafiq K, Kolpakov MA, Guo J, Koch WJ, et al. Beta1-adrenergic receptors promote focal adhesion signaling downregulation and myocyte apoptosis in acute volume overload. J Mol Cell Cardiol 2012;53:240–9. https://doi.org/10.1016/J.YJMCC.2012.05.004.

[15] Sabri A, Rafiq K, Seqqat R, Kolpakov MA, Dillon R, Dell'italia LJ. Sympathetic activation causes focal adhesion signaling alteration in early compensated volume overload attributable to isolated

746 mitral regurgitation in the dog. Circ Res 2008;102:1127–36.
747 https://doi.org/10.1161/CIRCRESAHA.107.163642.

748 [16] Pat B, Killingsworth C, Denney T, Zheng J, Powell P, Tillson M, et al. Dissociation between
749 cardiomyocyte function and remodeling with β-adrenergic receptor blockade in isolated canine
750 mitral regurgitation. Am J Physiol Heart Circ Physiol 2008;295:2321–7.
751 https://doi.org/10.1152/AJPHEART.00746.2008/ASSET/IMAGES/LARGE/ZH40120886060005.JPE
752 G.

753 [17] Zheng J, Chen Y, Pat B, Dell'Italia DLA, Tillson M, Dillon AR, et al. Molecular cardiology microarray
754 identifies extensive downregulation of noncollagen extracellular matrix and profibrotic growth
755 factor genes in chronic isolated mitral regurgitation in the dog. Circulation 2009;119:2086–95.
756 https://doi.org/10.1161/CIRCULATIONAHA.108.826230.

757 [18] Mohamed BA, Schnelle M, Khadjeh S, Lbik D, Herwig M, Linke WA, et al. Molecular and structural
758 transition mechanisms in long-term volume overload. Eur J Heart Fail 2016;18:362–71.
759 https://doi.org/10.1002/EJHF.465.

760 [19] Zeigler AC, Chandrabhatla AS, Christiansen SL, Nelson AR, Holmes JW, Saucerman JJ. Network
761 model-based screen for FDA-approved drugs affecting cardiac fibrosis. CPT Pharmacometrics Syst
762 Pharmacol 2021;10:377–88. https://doi.org/10.1002/PSP4.12599.

763 [20] Frank DU, Sutcliffe MD, Saucerman JJ. Network-based predictions of in vivo cardiac hypertrophy.
764 J Mol Cell Cardiol 2018;121:180–9. https://doi.org/10.1016/j.yjmcc.2018.07.243.

765 [21] Ross J, Sonnenblick EH, Taylor RR, Spotnitz HM, Covell JW. Diastolic Geometry and Sarcomere
766 Lengths in the Chronically Dilated Canine Left Ventricle. Circ Res 1971;28:49–61.
767 https://doi.org/10.1161/01.RES.28.1.49.

768 [22] Santamore WP, Burkhoff D. Hemodynamic consequences of ventricular interaction as assessed
769 by model analysis. American Journal of Physiology-Heart and Circulatory Physiology
770 1991;260:H146–57. https://doi.org/10.1152/ajpheart.1991.260.1.H146.

771 [23] Witzenburg CM, Holmes JW. Predicting the Time Course of Ventricular Dilation and Thickening
772 Using a Rapid Compartmental Model. J Cardiovasc Transl Res 2018;11:109–22.
773 https://doi.org/10.1007/S12265-018-9793-1.

774 [24] Dillon AR, Dell'Italia LJ, Tillson M, Killingsworth C, Denney T, Hathcock J, et al. Left ventricular
775 remodeling in preclinical experimental mitral regurgitation of dogs. Journal of Veterinary
776 Cardiology 2012;14:73–92. https://doi.org/10.1016/j.jvc.2012.01.012.

777 [25] Trappanese DM, Liu Y, McCormick RC, Cannavo A, Nanayakkara G, Baskharoun MM, et al.
778 Chronic β1-adrenergic blockade enhances myocardial β3-adrenergic coupling with nitric oxide-
779 cGMP signaling in a canine model of chronic volume overload: new insight into mechanisms of
780 cardiac benefit with selective β1-blocker therapy. Basic Res Cardiol 2015;110:456.
781 https://doi.org/10.1007/s00395-014-0456-3.

782 [26] Perry GJ, Wei CC, Hankes GH, Dillon SR, Rynders P, Mukherjee R, et al. Angiotensin II receptor
783 blockade does not improve left ventricular function andremodeling in subacute mitral

784 regurgitation in the dog. J Am Coll Cardiol 2002;39:1374–9. https://doi.org/10.1016/S0735-
785 1097(02)01763-1.

786 [27] Fomovsky GM, Clark SA, Parker KM, Ailawadi G, Holmes JW. Anisotropic reinforcement of acute
787 anteroapical infarcts improves pump function. Circ Heart Fail 2012;5:515–22.
788 https://doi.org/10.1161/CIRCHEARTFAILURE.111.965731.

789 [28] Spotnitz HM, Sonnenblick EH, Spiro D. Relation of Ultrastructure to Function in the Intact Heart:
790 Sarcomere Structure Relative to Pressure Volume Curves of Intact Left Ventricles of Dog and Cat.
791 Circ Res 1966;18:49–66. https://doi.org/10.1161/01.RES.18.1.49.

792 [29] Ryall KA, Holland DO, Delaney KA, Kraeutler MJ, Parker AJ, Saucerman JJ. Network reconstruction
793 and systems analysis of cardiac myocyte hypertrophy signaling. Journal of Biological Chemistry
794 2012;287:42259–68. https://doi.org/10.1074/jbc.M112.382937.

795 [30] Khalilimeybodi A, Paap AM, Christiansen SLM, Saucerman JJ. Context-specific network modeling
796 identifies new crosstalk in β-adrenergic cardiac hypertrophy. PLoS Comput Biol
797 2020;16:e1008490. https://doi.org/10.1371/journal.pcbi.1008490.

798 [31] Clark AP, Chowkwale M, Paap A, Dang S, Saucerman JJ. Logic-based modeling of biological
799 networks with Netflux. BioRxiv 2024:2024.01.11.575227.
800 https://doi.org/10.1101/2024.01.11.575227.

801 [32] Efendiev Y, Hou T, Luo W. Preconditioning Markov Chain Monte Carlo Simulations Using Coarse-
802 Scale Models. Https://DoiOrg/101137/050628568 2006;28:776–803.
803 https://doi.org/10.1137/050628568.

804 [33] Dhamala J, Arevalo HJ, Sapp J, Horácek BM, Wu KC, Trayanova NA, et al. Quantifying the
805 uncertainty in model parameters using Gaussian process-based Markov chain Monte Carlo in
806 cardiac electrophysiology. Med Image Anal 2018;48:43–57.
807 https://doi.org/10.1016/J.MEDIA.2018.05.007.

808 [34] Matsuo T, Carabello BA, Nagatomo Y, Koide M, Hamawaki M, Zile MR, et al. Mechanisms of
809 cardiac hypertrophy in canine volume overload. Am J Physiol Heart Circ Physiol 1998;275.
810 https://doi.org/10.1152/AJPHEART.1998.275.1.H65/ASSET/IMAGES/LARGE/AHEA40711007X.JPE
811 G.

812 [35] Dostal DE, Baker KM. Angiotensin II Stimulation of Left Ventricular Hypertrophy in Adult Rat
813 HeartMediation by the AT1 Receptor. Am J Hypertens 1992;5:276–80.
814 https://doi.org/10.1093/AJH/5.5.276.

815 [36] Dilley RJ, Nataatmadja I M. Heparin inhibits mesenteric vascular hypertrophy in angiotensin II-
816 infusion hypertension in rats. Cardiovasc Res 1998;38:247–55. https://doi.org/10.1016/S0008-
817 6363(98)00004-2/2/38-1-247-FIG5.GIF.

818 [37] Laks MM, Morady F, Swan HJC. Myocardial Hypertrophy Produced by Chronic Infusion of
819 Subhypertensive Doses of Norepinephrine in the Dog. Chest 1973;64:75–8.
820 https://doi.org/10.1378/chest.64.1.75.

821 [38] King BD, Sack D, Kichuk MR, Hintze TH. Absence of hypertension despite chronic marked
822 elevations in plasma norepinephrine in conscious dogs. Hypertension 1987;9:582–90.
823 https://doi.org/10.1161/01.HYP.9.6.582.

824 [39] Stewart JM, Patel MB, Wang J, Ochoa M, Gewitz M, Loud A V., et al. Chronic elevation of
825 norepinephrine in conscious dogs produces hypertrophy with no loss of LV reserve.
826 Https://DoiOrg/101152/Ajpheart19922622H331 1992;262:331–9.
827 https://doi.org/10.1152/AJPHEART.1992.262.2.H331.

828 [40] Estrada AC, Yoshida K, Saucerman JJ, Holmes JW. A multiscale model of cardiac concentric
829 hypertrophy incorporating both mechanical and hormonal drivers of growth. Biomech Model
830 Mechanobiol 2021;20:293–307. https://doi.org/10.1007/s10237-020-01385-6.

831 [41] Murray DB, McMillan R, Brower GL, Janicki JS. ETA selective receptor antagonism prevents
832 ventricular remodeling in volume-overloaded rats. Am J Physiol Heart Circ Physiol 2009;297:109–
833 16.
834 https://doi.org/10.1152/AJPHEART.00968.2008/ASSET/IMAGES/LARGE/ZH40070989120006.JPE
835 G.

836 [42] Francis B, Winaver J, Karram T, Hoffman A, Abassi Z. Renal and systemic effects of chronic
837 blockade of ETA or ET B in normal rats and animals with experimental heart failure. J Cardiovasc
838 Pharmacol 2004;44. https://doi.org/10.1097/01.FJC.0000166214.42791.F2.

839 [43] Lee DS, Kim DK, Choi SM, Kim YK, Ko BH, Jung YW. Bosentan Attenuates Compensatory Left
840 Ventricular Hypertrophy Induced by Aortocaval Fistula in Rats. Korean Circ J 2005;35:665.
841 https://doi.org/10.4070/kcj.2005.35.9.665.

842 [44] Lüscher TF, Enseleit F, Pacher R, Mitrovic V, Schulze MR, Willenbrock R, et al. Hemodynamic and
843 neurohumoral effects of selective endothelin A (ETA) receptor blockade in chronic heart failure:
844 The heart failure ETA receptor blockade trial (HEAT). Circulation 2002;106:2666–72.
845 https://doi.org/10.1161/01.CIR.0000038497.80095.E1/ASSET/D1290F76-5B32-4F11-A37D-
846 58DB5407C8B6/ASSETS/GRAPHIC/G12FF1.JPEG.

847 [45] Murray DB, Gardner JD, Brower GL, Janicki JS. Effects of nonselective endothelin-1 receptor
848 antagonism on cardiac mast cell-mediated ventricular remodeling in rats. Am J Physiol Heart Circ
849 Physiol 2008;294:1251–7.
850 https://doi.org/10.1152/AJPHEART.00622.2007/ASSET/IMAGES/LARGE/ZH40030881090005.JPE
851 G.

852 [46] Zhang W, Elimban V, Xu YJ, Zhang M, Nijjar MS, Dhalla NS. Alterations of Cardiac ERK1/2
853 Expression and Activity Due to Volume Overload Were Attenuated by the Blockade of RAS.
854 Https://DoiOrg/101177/1074248409356430 2010;15:84–92.
855 https://doi.org/10.1177/1074248409356430.

856 [47] Yoshida K, Holmes JW. Computational models of cardiac hypertrophy. Prog Biophys Mol Biol
857 2021;159:75–85. https://doi.org/10.1016/J.PBIOMOLBIO.2020.07.001.

858 [48] Caggiano LR, Holmes JW, Witzenburg CM. Individual variability in animal-specific hemodynamic
859 compensation following myocardial infarction. J Mol Cell Cardiol 2022;163:156–66.
860 https://doi.org/10.1016/j.yjmcc.2021.10.008.

861 [49] Freire G, Ocampo C, Ilbawi N, Griffin AJ, Gupta M. Overt expression of AP-1 reduces alpha myosin
862 heavy chain expression and contributes to heart failure from chronic volume overload. J Mol Cell
863 Cardiol 2007;43:465–78. https://doi.org/10.1016/J.YJMCC.2007.07.046.

864 [50] Lachance D, Dhahri W, Drolet MC, Roussel É, Gascon S, Sarrhini O, et al. Endurance training or
865 beta-blockade can partially block the energy metabolism remodeling taking place in experimental
866 chronic left ventricle volume overload. BMC Cardiovasc Disord 2014;14:1–11.
867 https://doi.org/10.1186/1471-2261-14-190/FIGURES/8.

868 [51] Fareh J, Touyz RM, Schiffrin EL, Thibault G. Endothelin-1 and Angiotensin II Receptors in Cells
869 From Rat Hypertrophied Heart. Circ Res 1996;78:302–11.
870 https://doi.org/10.1161/01.RES.78.2.302.

871 [52] Urabe Y, Mann DL, Kent RL, Nakano K, Tomanek RJ, Carabello BA, et al. Cellular and ventricular
872 contractile dysfunction in experimental canine mitral regurgitation. Circ Res 1992;70:131–47.
873 https://doi.org/10.1161/01.RES.70.1.131.

874 [53] Kala P, Gawrys O, Miklovič M, Vaňourková Z, Škaroupková P, Jíchová Š, et al. Endothelin type A
875 receptor blockade attenuates aorto-caval fistula-induced heart failure in rats with angiotensin II-
876 dependent hypertension. J Hypertens 2023;41:99–114.
877 https://doi.org/10.1097/HJH.0000000000003307.

878 [54] Dell'Italia LJ, Balcells E, Meng QC, Su X, Schultz D, Bishop SP, et al. Volume-overload cardiac
879 hypertrophy is unaffected by ACE inhibitor treatment in dogs.
880 Https://DoiOrg/101152/Ajpheart19972732H961 1997;273:961–70.
881 https://doi.org/10.1152/AJPHEART.1997.273.2.H961.

882 [55] Tallaj J, Wei C-C, Hankes GH, Holland M, Rynders P, Dillon AR, et al. β_1-Adrenergic Receptor
883 Blockade Attenuates Angiotensin II–Mediated Catecholamine Release Into the Cardiac
884 Interstitium in Mitral Regurgitation. Circulation 2003;108:225–30.
885 https://doi.org/10.1161/01.CIR.0000079226.48637.5A.

886 [56] Leskinen H, Vuolteenaho O, Ruskoaho H. Combined Inhibition of Endothelin and Angiotensin II
887 Receptors Blocks Volume Load–Induced Cardiac Hormone Release. Circ Res 1997;80:114–23.
888 https://doi.org/10.1161/01.RES.80.1.114.

889 [57] Enevoldsen FC, Sahana J, Wehland M, Grimm D, Infanger M, Krüger M. Endothelin Receptor
890 Antagonists: Status Quo and Future Perspectives for Targeted Therapy. Journal of Clinical
891 Medicine 2020, Vol 9, Page 824 2020;9:824. https://doi.org/10.3390/JCM9030824.

892 [58] Nemoto S, Hamawaki M, De Freitas G, Carabello BA. differential effects of the angiotensin-
893 converting enzyme inhibitor lisinopril versus the beta-adrenergic receptor blocker atenolol on
894 hemodynamics and left ventricular contractile function in experimental mitral regurgitation. J Am
895 Coll Cardiol 2002;40:149–54. https://doi.org/10.1016/S0735-1097(02)01926-5.

896 [59] Tsutsui H, Spinale FG, Nagatsu M, Schmid PG, Ishihara K, DeFreyte G, et al. Effects of chronic
897 beta-adrenergic blockade on the left ventricular and cardiocyte abnormalities of chronic canine
898 mitral regurgitation. Journal of Clinical Investigation 1994;93:2639–48.
899 https://doi.org/10.1172/JCI117277.

900 [60] Nagatsu M, Zile MR, Tsutsui H, Schmid PG, DeFreyte G, Cooper IV G, et al. Native beta-adrenergic
901 support for left ventricular dysfunction in experimental mitral regurgitation normalizes indexes of
902 pump and contractile function. Circulation 1994;89:818–26.
903 https://doi.org/10.1161/01.CIR.89.2.818.

904 [61] Gao Y, Arfat Y, Wang H, Goswami N. Muscle atrophy induced by mechanical unloading:
905 Mechanisms and potential countermeasures. Front Physiol 2018;9:324534.
906 https://doi.org/10.3389/FPHYS.2018.00235/BIBTEX.

907 [62] Wisdom KM, Delp SL, Kuhl E. Use it or lose it: multiscale skeletal muscle adaptation to mechanical
908 stimuli. Biomech Model Mechanobiol 2015;14:195–215. https://doi.org/10.1007/s10237-014-
909 0607-3.

910 [63] Peng X, Kraus MS, Wei H, Shen TL, Pariaut R, Alcaraz A, et al. Inactivation of focal adhesion kinase
911 in cardiomyocytes promotes eccentric cardiac hypertrophy and fibrosis in mice. J Clin Invest
912 2006;116:217–27. https://doi.org/10.1172/JCI24497.

913

914

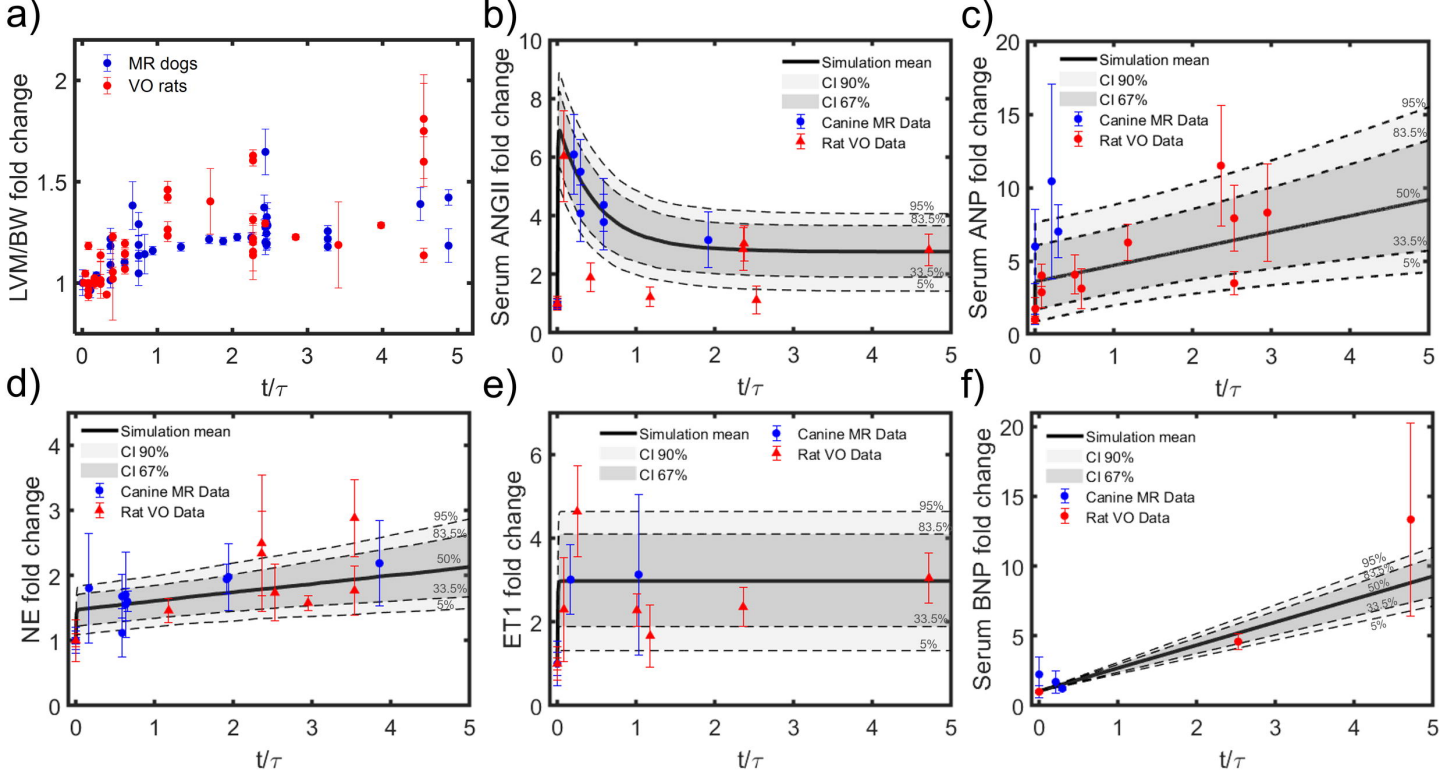
a)
MR dogs
VO rats
LVMI/BW fold change
t/τ
b)
Simulation mean
CI 90%
CI 67%
Canine MR Data
Rat VO Data
Serum ANGII fold change
95%
83.5%
33.5%
5%
t/τ
c)
Simulation mean
CI 90%
CI 67%
Canine MR Data
Rat VO Data
Serum ANP fold change
95%
83.5%
50%
33.5%
5%
t/τ
d)
Simulation mean
CI 90%
CI 67%
Canine MR Data
Rat VO Data
NE fold change
95%
83.5%
50%
33.5%
5%
t/τ
e)
Simulation mean
CI 90%
CI 67%
Canine MR Data
Rat VO Data
ET1 fold change
95%
83.5%
33.5%
5%
t/τ
f)
Simulation mean
CI 90%
CI 67%
Canine MR Data
Rat VO Data
Serum BNP fold change
95%
83.5%
50%
33.5%
5%
t/τ

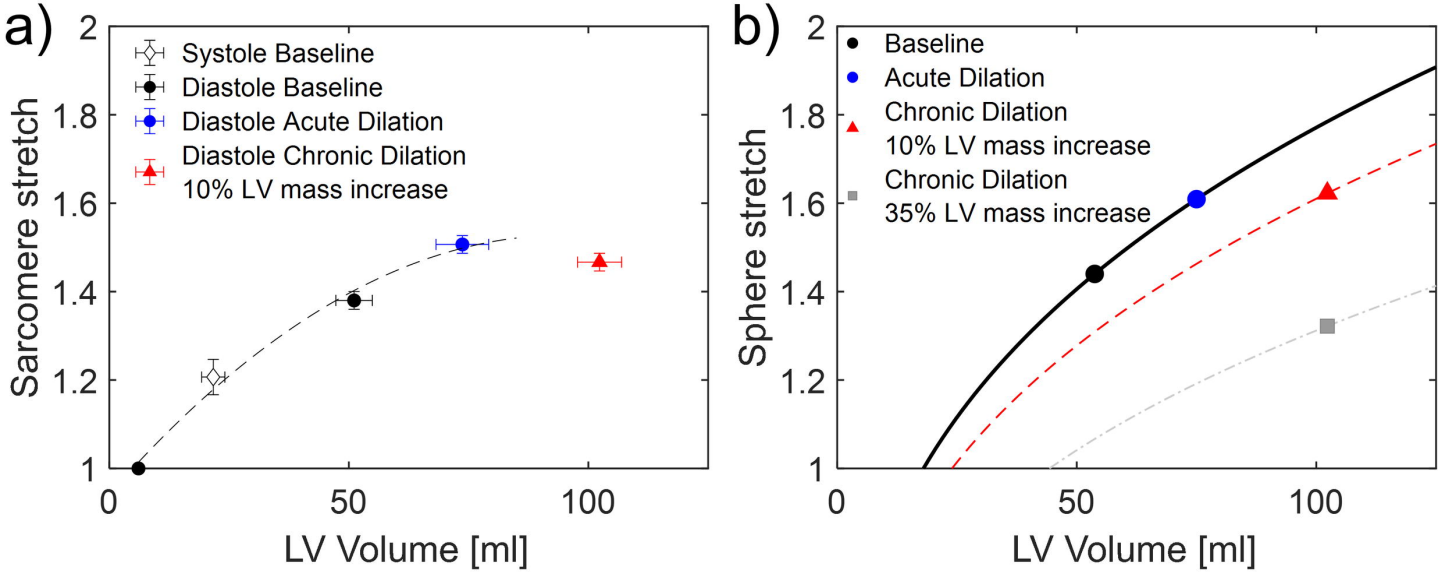
a)
Systole Baseline
Diastole Baseline
Diastole Acute Dilation
Diastole Chronic Dilation
10% LV mass increase
Sarcomere stretch
LV Volume [ml]
b)
Baseline
Acute Dilation
Chronic Dilation
10% LV mass increase
Chronic Dilation
35% LV mass increase
Sphere stretch
LV Volume [ml]

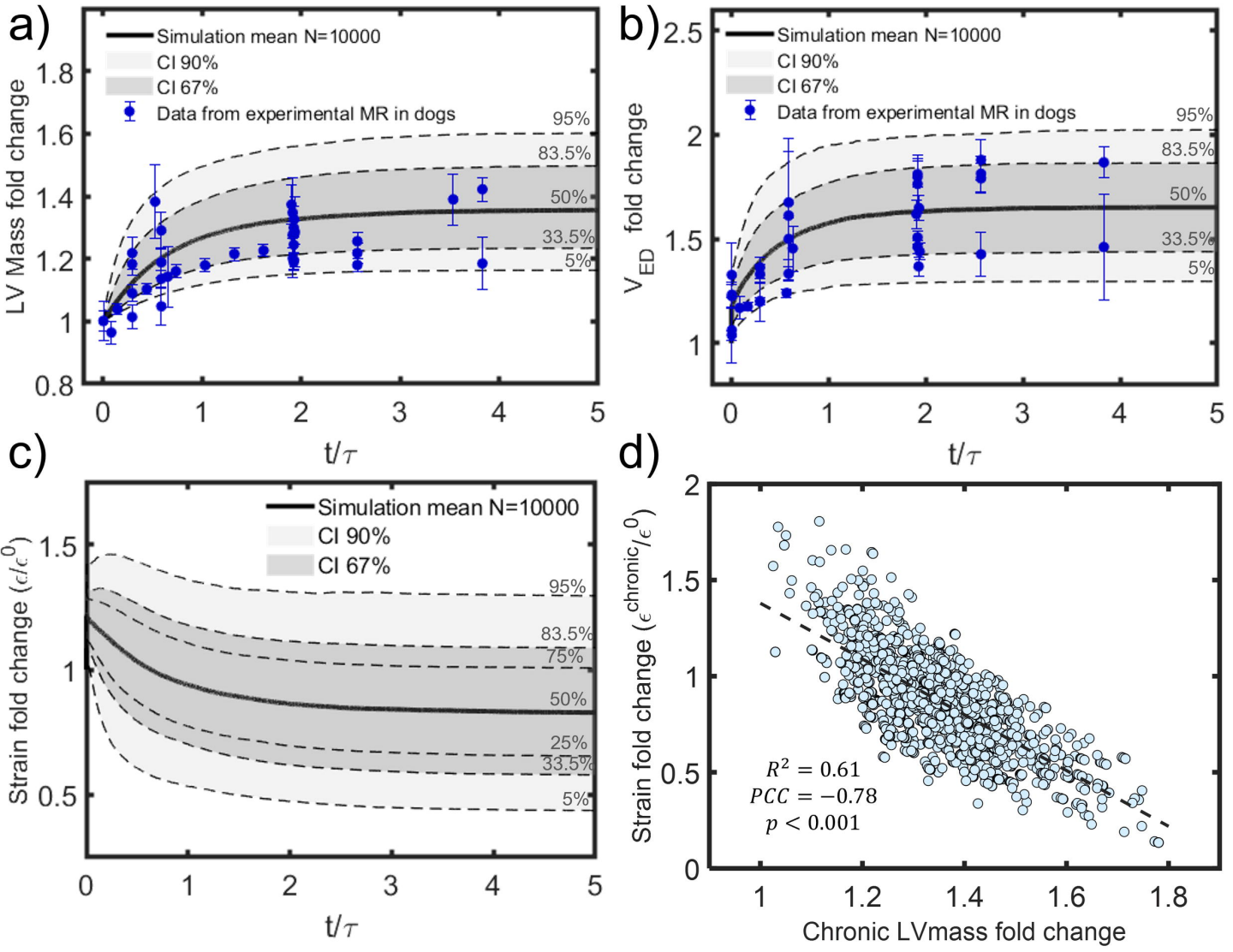
a)
Simulation mean N=10000
CI 90%
CI 67%
Data from experimental MR in dogs
95%
83.5%
50%
33.5%
5%
LV Mass fold change
t/τ
b)
Simulation mean N=10000
CI 90%
CI 67%
Data from experimental MR in dogs
95%
83.5%
50%
33.5%
5%
V_ED fold change
t/τ
c)
Simulation mean N=10000
CI 90%
CI 67%
95%
83.5%
75%
50%
25%
33.5%
5%
Strain fold change (ε/ε^0)
t/τ
d)
R^2 = 0.61
PCC = −0.78
p < 0.001
Strain fold change (ε^chronic/ε^0)
Chronic LVmass fold change

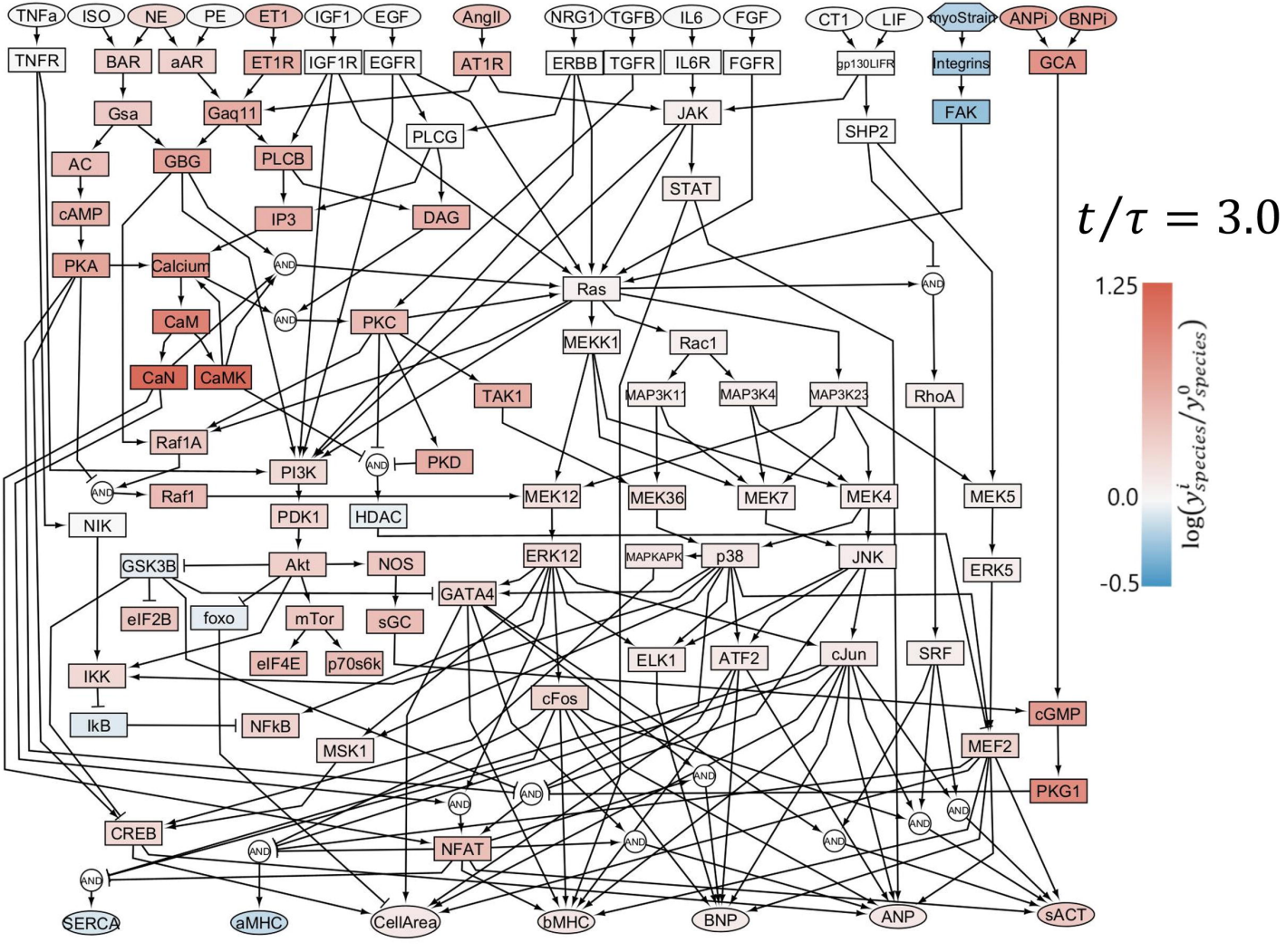
TNFa
ISO
NE
PE
ET1
IGF1
EGF
AngII
NRG1
TGFB
IL6
FGF
CT1
LIF
myoStrain
ANPi
BNPi
TNFR
BAR
aAR
ET1R
IGF1R
EGFR
AT1R
ERBB
TGFR
IL6R
FGFR
gp130LIFR
Integrins
GCA
Gsa
Gaq11
JAK
FAK
PLCG
SHP2
AC
GBG
PLCB
STAT
cAMP
IP3
DAG
PKA
Calcium
AND
Ras
CaM
PKC
MEKK1
Rac1
CaN
CaMK
TAK1
MAP3K11
MAP3K4
MAP3K23
RhoA
Raf1A
PI3K
PKD
Raf1
MEK12
MEK36
MEK7
MEK4
MEK5
NIK
PDK1
HDAC
GSK3B
Akt
NOS
ERK12
MAPKAPK
p38
JNK
ERK5
GATA4
eIF2B
foxo
mTor
sGC
eIF4E
p70s6k
ELK1
ATF2
cJun
SRF
IKK
cFos
cGMP
IkB
NFkB
MSK1
MEF2
PKG1
CREB
NFAT
SERCA
aMHC
CellArea
bMHC
BNP
ANP
sACT
$t/\tau = 3.0$
1.25
0.0
-0.5
$\log(y^i_{species}/y^0_{species})$

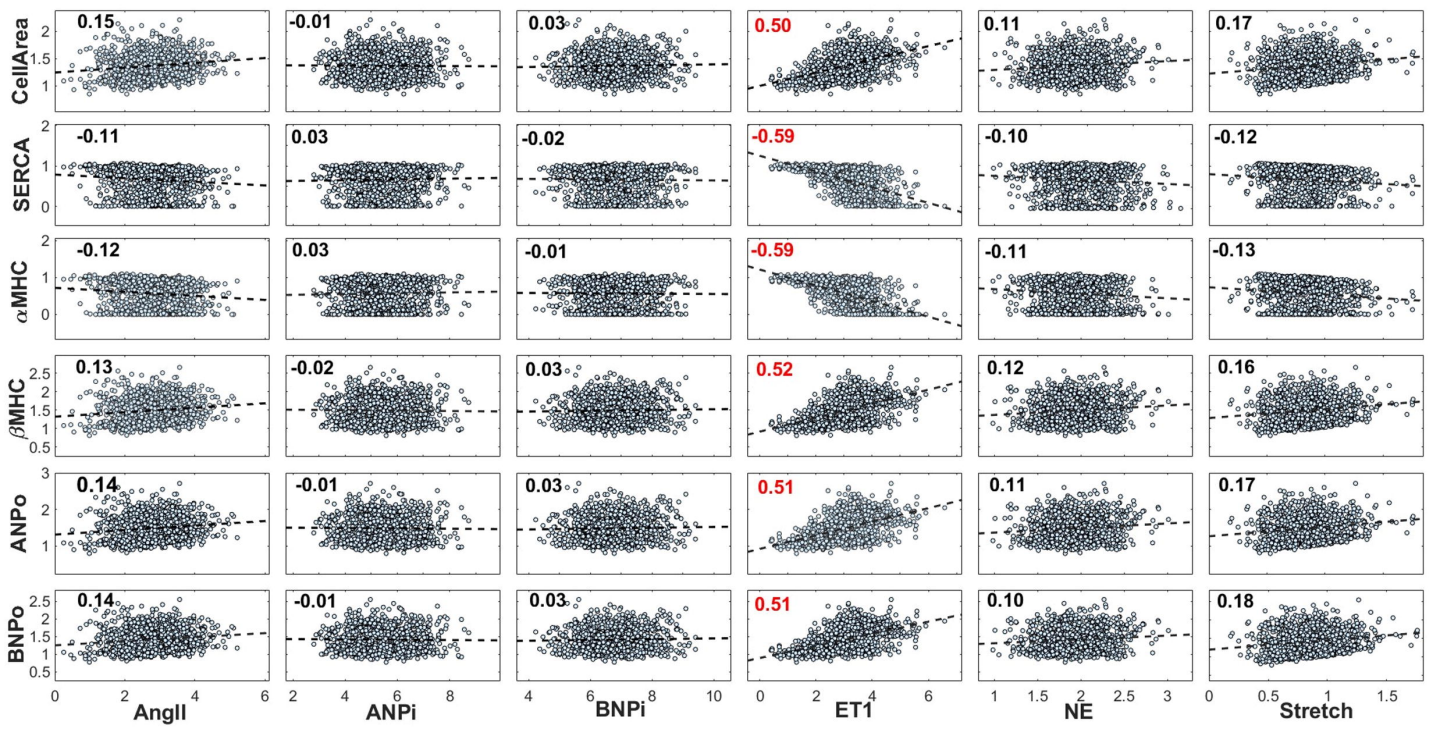
CellArea
SERCA
αMHC
βMHC
ANPo
BNPo
AngII
ANPi
BNPi
ET1
NE
Stretch
0.15
-0.01
0.03
0.50
0.11
0.17
-0.11
0.03
-0.02
-0.59
-0.10
-0.12
-0.12
0.03
-0.01
-0.59
-0.11
-0.13
0.13
-0.02
0.03
0.52
0.12
0.16
0.14
-0.01
0.03
0.51
0.11
0.17
0.14
-0.01
0.03
0.51
0.10
0.18

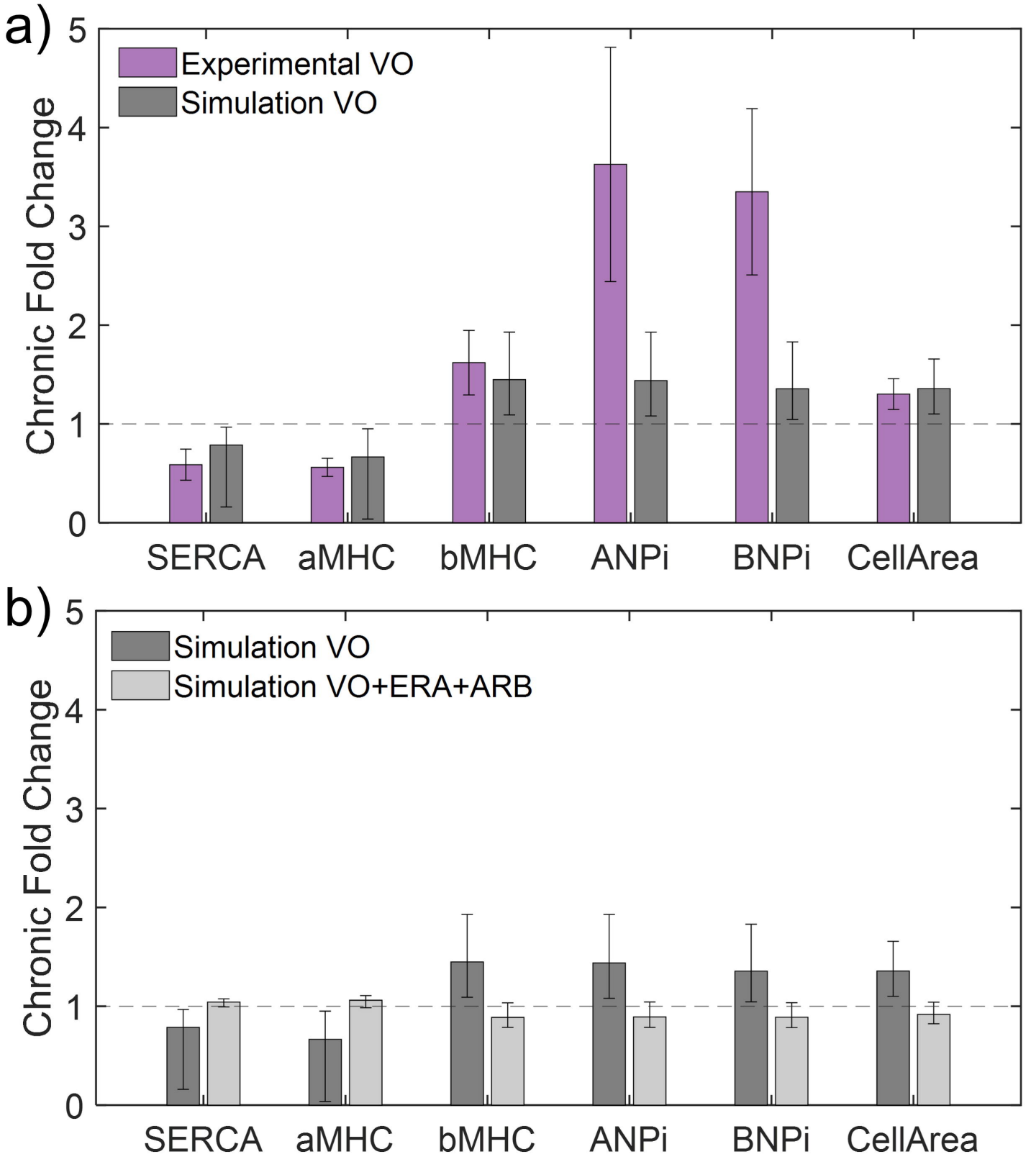
a)
Experimental VO
Simulation VO
Chronic Fold Change
0
1
2
3
4
5
SERCA
aMHC
bMHC
ANPi
BNPi
CellArea
b)
Simulation VO
Simulation VO+ERA+ARB
Chronic Fold Change
0
1
2
3
4
5
SERCA
aMHC
bMHC
ANPi
BNPi
CellArea

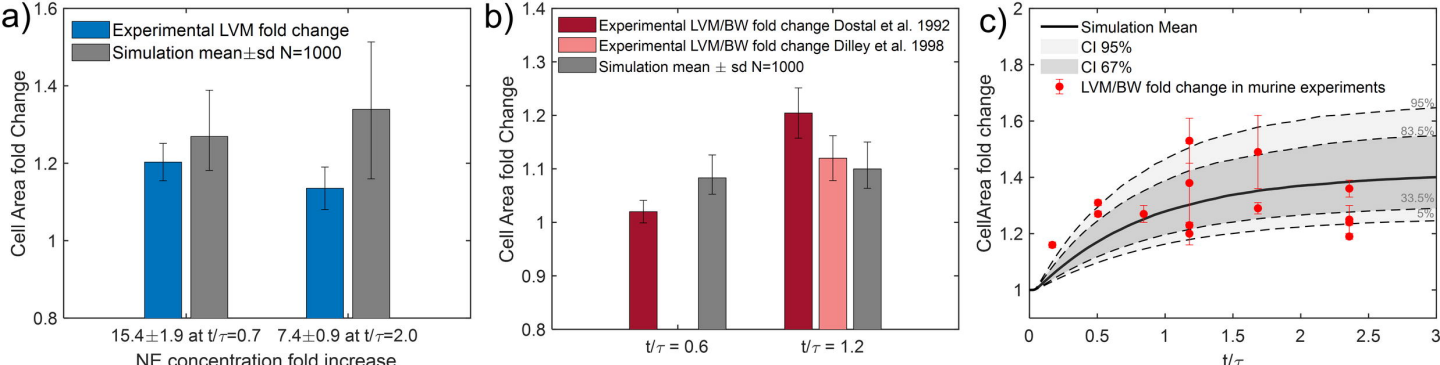
a)
Experimental LVM fold change
Simulation mean±sd N=1000
Cell Area fold Change
1.6
1.4
1.2
1
0.8
15.4±1.9 at t/τ=0.7
7.4±0.9 at t/τ=2.0
NE concentration fold increase
b)
Experimental LVM/BW fold change Dostal et al. 1992
Experimental LVM/BW fold change Dilley et al. 1998
Simulation mean ± sd N=1000
Cell Area fold Change
1.4
1.3
1.2
1.1
1
0.9
0.8
t/τ = 0.6
t/τ = 1.2
c)
Simulation Mean
CI 95%
CI 67%
LVM/BW fold change in murine experiments
95%
83.5%
33.5%
5%
CellArea fold change
2
1.8
1.6
1.4
1.2
1
0
0.5
1
1.5
2
2.5
3
t/τ

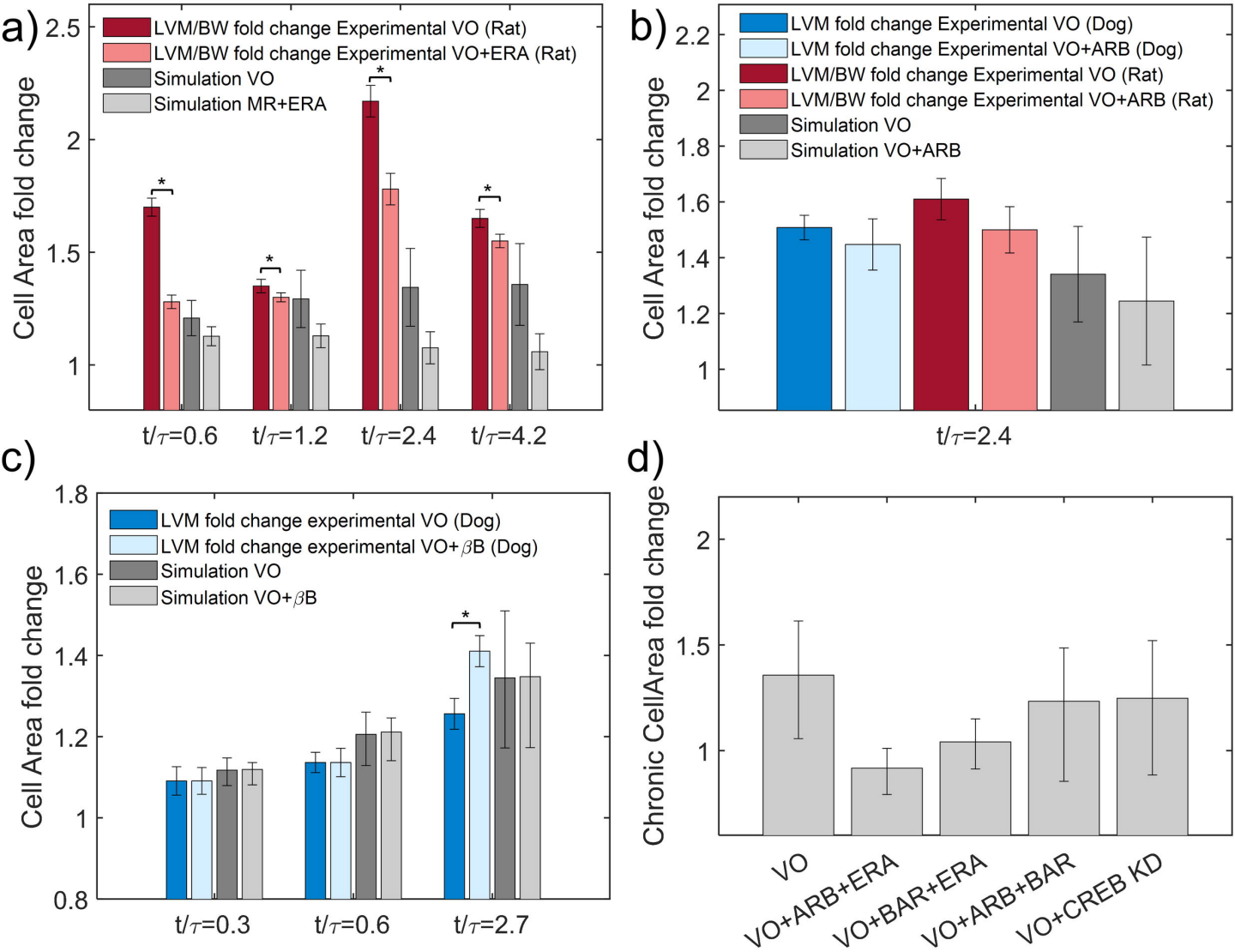
a)
LVM/BW fold change Experimental VO (Rat)
LVM/BW fold change Experimental VO+ERA (Rat)
Simulation VO
Simulation MR+ERA
Cell Area fold change
2.5
2
1.5
1
*
t/τ=0.6
t/τ=1.2
t/τ=2.4
t/τ=4.2
b)
LVM fold change Experimental VO (Dog)
LVM fold change Experimental VO+ARB (Dog)
LVM/BW fold change Experimental VO (Rat)
LVM/BW fold change Experimental VO+ARB (Rat)
Simulation VO
Simulation VO+ARB
Cell Area fold change
2.2
2
1.8
1.6
1.4
1.2
1
t/τ=2.4
c)
LVM fold change experimental VO (Dog)
LVM fold change experimental VO+βB (Dog)
Simulation VO
Simulation VO+βB
Cell Area fold change
1.8
1.6
1.4
1.2
1
0.8
*
t/τ=0.3
t/τ=0.6
t/τ=2.7
d)
Chronic CellArea fold change
2
1.5
1
VO
VO+ARB+ERA
VO+BAR+ERA
VO+ARB+BAR
VO+CREB KD